Deficient endoplasmic reticulum-mitochondrial phosphatidylserine transfer causes liver disease

María Isabel Hernández-Alvarez[1,3,11*], David Sebastián[1,2,3], Sara Vives [1], Saška Ivanova[1,2,3], Paola Bartoccioni[1,2,4], Pamela Kakimoto [1], Natalia Plana[1], Sónia R. Veiga[5], Vanessa Hernández[1], Nuno Vasconcelos[1], Peddinti Gopalacharyulu[6], Anna Adrover[1], Mariona Jové [13], Reinald Pamplona [13], Antonio Berenguer-Llergo[1], Isabel Gordaliza[1,2,3], Enrique Calvo[11],Noemí Cabré[12], Rui Castro[7], Antonija Kuzmanic [1], Marie Boutant[8], David Sala[1,2,3], Tuulia Hyotylainen[9], Matej Orešič[10], Joana Fort[1,2,4], Ekaitz Errasti-Murugarren[1,4], Modesto Orozco [1],Jorge Joven[12], Carles Cantó[8], Manuel Palacin[1,2,4], Sonia Fernández-Veledo[3,11], Joan Vendrell[3,11] and Antonio Zorzano[1,2,3*]

[1]Institute for Research in Biomedicine (IRB Barcelona). The Barcelona Institute of Science and Technology, Barcelona, Spain;

[2]Departament de Bioquímica i Biomedicina Molecular, Facultat de Biologia, 08028 Barcelona, Spain;

[3]CIBER de Diabetes y Enfermedades Metabólicas Asociadas (CIBERDEM), Instituto de Salud Carlos III;

[4]CIBERER, Instituto de Salud Carlos III, Spain;

[5] Cancer Metabolism Group, ONCOBELL Program, Bellvitge Biomedical Research Institute (IDIBELL), Barcelona, Spain;

[6]Institute for Molecular Medicine Finland (FIMM) Nordic EMBL Partnership for Molecular Medicine Biomedicum, University of Helsinki Finland;

[7]Research Institute for Medicines (iMed.ULisboa), and Department of Biochemistry and Human Biology, Faculty of Pharmacy, Universidade de Lisboa, 1649-003 Lisboa, Portugal;

[8]Nestlé Institute of Health Sciences SA, Lausanne (Switzerland);

[9]Department of Chemistry, University of Örebro, Örebro, Sweden;

[10]Turku Centre for Biotechnology, University of Turku and Åbo Akademi University, Turku, Finland;

[11]Hospital Universitari de Tarragona Joan XXIII, Institut Investigació Sanitaria Pere Virgili, Universitat Rovira i Virgili, Tarragona, Spain.

[12]Biochemical Research Unit, Hospital Universitari de Sant Joan, Institut d'Investigació Sanitària Pere Virgili, Universitat Rovira i Virgili, C. Sant Joan s/n, Reus, 43201, Spain

*Corresponding author. Institute for Research in Biomedicine, C/ Baldiri Reixac 10, 08028 Barcelona. Tel:+34-934037197; Fax:+34-934034717; E-mail: antonio.zorzano@irbbarcelona.org; misabel.hernandez.alvarez@gmail.com

The authors declare no conflict of interest. CC and MB are employees of the Nestlé Institute of Health Sciences S.A.

Summary

Non-alcoholic fatty liver disease is the most common liver disease worldwide. Here, we show that the mitochondrial protein mitofusin 2 (Mfn2) protects against liver disease. Reduced Mfn2 expression was detected in liver biopsies from patients with non-alcoholic steatohepatitis (NASH). Moreover, reduced Mfn2 expression was detected in mouse models of steatosis or NASH, and its re-expression in a NASH mouse model ameliorated the disease. Liver-specific ablation of Mfn2 in mice provoked inflammation, triglyceride accumulation, fibrosis and liver cancer. We demonstrate that Mfn2 binds phosphatidylserine (PS) and can specifically extract PS into membrane domains, favoring PS transfer to mitochondria, as well as mitochondrial phosphatidylethanolamine (PE) synthesis. Consequently, hepatic Mfn2 deficiency reduces PS transfer and phospholipid synthesis, leading to endoplasmic reticulum (ER) stress and the development of a NASH-like phenotype and liver cancer. Thus, ablation of Mfn2 in liver reveals that disruption of ER-mitochondrial PS transfer is a new mechanism involved in the development of liver disease.

Introduction

Non-alcoholic fatty liver disease (NAFLD) is among the most common liver diseases worldwide, with increasing prevalence in parallel with the obesity/metabolic syndrome epidemic. NAFLD represents a clinical spectrum ranging from simple steatosis and non-alcoholic steatohepatitis (NASH) to cirrhosis and hepatocellular carcinoma (HCC)[1]. NASH is accompanied by inflammation, cell death, and fibrosis, and is characterized histologically by the presence of ballooning hepatocytes and lobular inflammation with or without perisinusoidal fibrosis and steatosis[2]. Hepatic inflammation is a complex process that originates in response to a variety of stress conditions[3]. In the course of the inflammatory process, liver hepatocytes frequently die by programmed cell death. The persistent cycle of "necro-inflammation" and hepatocyte regeneration is believed to enhance the risk of genetic mutation in hepatocytes, promoting survival and expansion of initiated cells. The result is increased cell growth, also referred to as compensatory proliferation, which can lead to tumor development[4,5]. In this context, epidemiological and clinical studies have provided convincing evidence that chronic inflammation leads to carcinogenesis[6-9].

Several potential factors influencing NASH progression are known to interact[10-15], such as hepatic endoplasmic reticulum (ER) stress, oxidative stress, mitochondrial dysfunction and lipotoxicity. Mitochondrial function is governed by the preservation of a normal lipid composition[16-19], which is dependent on the capacity of mitochondria to synthesize phospholipids, and by the traffic of lipids from the ER to mitochondria[20-22]. Specifically, phosphatidylserine (PS) is primarily synthesized in the ER and is imported into mitochondria by transient membrane contact between mitochondria-associated ER membranes (MAMs) and the mitochondrial outer membrane[23]. In mitochondria, PS is converted into phosphatidylethanolamine (PE), which is then imported into the ER for conversion to phosphatidylcholine (PC)[16,21,24,25]. Accordingly, MAMs are key sites for synthesis and traffic of phospholipids[17,25].

Mitofusin 2 (Mfn2) is a mitochondrial membrane protein with a role connecting ER membranes to mitochondria[26-28], and its depletion causes ER stress[29-31]. Mfn2 plays a relevant role in the maintenance of mitochondrial metabolism, insulin signaling and energy homeostasis[30-33]. Cancer cells of different origin show a low expression of Mfn2 [34-37]. In addition, Mfn2 levels are significantly downregulated in HCC tissue compared

with corresponding adjacent normal tissue, and there is a negative correlation between Mfn2 levels and the prognosis of cancer[38-40]. Mfn2 overexpression in hepatocellular carcinoma or colorectal cancer cells reduces cell proliferation and induces spontaneous apoptosis[35,37]. However, it is unknown whether Mfn2 downregulation is a cause or a consequence of cancer, and in addition, there are no data linking Mfn2 to NALFD progression.

Here we show that hepatic Mfn2 is downregulated both in patients with NASH, and in subjects borderline for NASH. Further, mouse models of hepatic lipid accumulation or NASH present lower levels of Mfn2 in liver, and the re-expression of Mfn2 in liver ameliorates the NASH phenotype. We also demonstrate that hepatic Mfn2 ablation causes a NASH-like phenotype that progresses to liver cancer with age. We show that Mfn2 binds to and participates in the transfer of PS. Accordingly, hepatic Mfn2 deficiency causes a reduced transfer of PS from ER to mitochondria, which leads to reduced PS synthesis and ER stress, in turn causing inflammation, fibrosis and liver cancer. Overall, our data strongly suggest that Mfn2 constitutes a new target for the treatment of NALFD.

Results

Human liver samples of non-alcoholic steatohepatitis present low levels of Mfn2

To investigate whether Mfn2 is dysregulated in NASH, we compared its expression in liver biopsies from patients with steatosis or NASH. Clinical, anthropometric, and biochemical data of this cohort have been reported previously[41]. Results showed that protein levels of Mfn2 were significantly lower in liver from patients with NASH than in subjects with simple steatosis (Figure 1A). We also analyzed human liver biopsies from a second cohort of subjects without NASH (NAS index $\leq$3) and close to borderline NASH (NAS index $\geq$5). NAS scoring was performed according Takeda et al.,[42]. Clinical characteristics of these patients are shown in Supplementary Table 1. Both Mfn2 mRNA and protein levels were significantly decreased in patients with borderline NASH (Figures S1A, S1B and S1C). By contrast, expression of the Mfn2 homologue Mfn1 was unaltered in this group (Figure S1D). Overall, these data show that Mfn2 is down-regulated in human liver during progression from steatosis to NASH.

Mouse models of non-alcoholic liver disease have low hepatic levels of Mfn2

To document the possible involvement of Mfn2 in NALFD, we studied its expression in C57BL6/J mice with steatosis induced by high-fat diet (HFD) over three weeks, a time sufficient to trigger hepatic steatosis[43]. Mfn2 protein expression in liver was significanly lower in the HFD group than in the control group (Figures 1B, and S1E). Because mice on HFD show fatty liver and obesity but not fibrosis[44], we utilized a well-established mouse model of NASH consisting of a methionine/choline-deficient diet combined with 45% HFD and supplemented with 0.1% L-methionine in drinking water, to avoid weight loss[44] (hereafter termed MCD). C57BL6/J mice on MCD diet for 3 weeks showed substantial fat accumulation and liver fibrosis (detected by H&E and Sirius Red staining, respectively) (Figure 1C). Further, liver triglyceride levels and mRNA levels of inflammatory markers and the fibrotic marker TGFβ were significantly higher in mice on MCD diet than on control diet (Figures 1D, S1F and S1G). Under these conditions Mfn2 levels were diminished (Figures 1E, and S1H), and this decrease was greater in mice on MCD diet than on HFD (Figure 1B and 1E). Consistent with the data in human biopsies, Mfn1 protein levels were unaltered in mice on MCD diet (Figure

S1I). These results are consistent with a specific progressive repression of Mfn2 in mouse liver disease.

Mfn2 ablation causes chronic hepatic inflammation and abnormal lipid metabolism

To substantiate the role of Mfn2 in liver as a trigger of the NASH-like phenotype, we analyzed liver-specific Mfn2 knockout mice (L-KO) generated in our laboratory[31]. Under normal chow diet, 8 week-old L-KO mice showed a significant increase in the abundance of hepatic and plasma pro-inflammatory cytokines (Figures 1F, S2A and S2B), expression of hepatic pro-inflammatory genes (Figure S2C) and a modest but significant accumulation of triglycerides (Figure 1G). This occurred in the absence of changes in body weight, food intake or circulating lipids (Figures S2D–H). Further analysis of lipid metabolism in hepatocytes isolated from L-KO and control mice revealed that the esterification of oleate into diacylglycerol and triacylglycerol was enhanced in the former, but their incorporation into phospholipids was decreased (Figure 1H). Under these conditions, oleate β-oxidation was decreased in Mfn2-deficient hepatocytes (Figure S2I). Further, the expression of *de novo* lipogenesis and esterification genes was modestly elevated in liver from L-KO mice (Figures S2J). In sum, L-KO mice show a pattern typical of disturbances in hepatic lipid metabolism.

Mfn2 ablation causes apoptosis, increased cell growth, fibrosis and liver cancer

It is known that chronic hepatic inflammation is associated with enhanced apoptosis, leading to compensatory cell proliferation and fibrosis, which are known risk factors for liver cancer[45,46]. Given the chronic inflammation detected in L-KO mice, we analyzed the development of these processes to determine whether Mfn2 deficiency leads to liver cancer progression. Under normal conditions, apoptosis was higher in liver from L-KO mice than from controls, as demonstrated by increased levels of cleaved PARP-1 and cleaved caspase-3 (Figures S3A and S3B), and was accompanied by a higher number of Ki67-positive cells (Figure S3C), indicating enhanced proliferation. Furthermore, the expression of genes encoding fibrotic markers was also elevated in L-KO livers (Figure 1J), and Sirius red staining and transmission electron microscopy revealed a marked accumulation of extracellular collagen in livers at 27 weeks of age (Figure 1I).

We next explored whether hepatic Mfn2 deficiency promotes liver cancer as a consequence of the natural progression of liver disease. Accordingly, L-KO and control mice on normal diet were examined for liver tumors at twenty-four months of age. Analysis showed that the number of tumors was significantly higher in L-KO mice than in control mice, and tumor volume was also greater (Figures 1K and S3D). We next sought to validate these results by investigating whether L-KO mice showed a differential predisposition to the liver-specific carcinogen diethylnitrosamine (DEN). Treatment of mice with DEN triggers a well-known cascade of events in liver that include DNA damage and apoptosis of centrilobular hepatocytes, production of proinflammatory cytokines and compensatory proliferation[47]. As a first approach, we induced liver DNA damage with a single high-dose intraperitoneal injection of DEN (50 mg/kg) to assess the acute liver response. Immunohistological examination of livers 48 h after DEN injection revealed a stronger DNA damage response in centrilobular regions in L-KO mice than in controls, and this accompanied by greater levels of compensatory proliferation (Figures S3E, S3F, and S3G). We next treated control and L-KO mice with a single lower dose of DEN (5 mg/kg), followed by continued exposure to HFD. After seven months L-KO mice subjected to DEN-HFD treatment showed a larger number of tumors and greater tumor size compared to control treated mice (Figure S3H). Thus, our data indicate that hepatic Mfn2 ablation leads to apoptosis, increased cell proliferation, fibrosis, and a greater susceptibility to develop liver cancer.

Mfn2 re-expression restores normal liver metabolism in L-KO mice

To assess whether the alterations detected in Mfn2-deficient livers were attributable to Mfn2 loss-of-function or to compensatory mechanisms, we re-expressed Mfn2 in L-KO mice by intravenous administration of adenoviruses encoding either Mfn2 or LacZ (AdC, used as a control). Upon Mfn2 re-expression (Figure S4A) hepatic and plasma cytokines returned to control levels (Figures S4B–D) and the expression of fibrosis genes and pro-inflammatory genes were markedly down-regulated (Figure S4E and S4G). Moreover, triacylglycerol levels were normalized (Figure S4F), and oleate β-oxidation was enhanced (Figure S4H).

We have previously reported that under normal chow diet, 8-week-old L-KO mice present an elevated unfolded protein response (UPR)[31]. Thus, we surveyed the impact of Mfn2 re-expression on ER stress markers. Results showed that Mfn2 re-expression normalized the different UPR parameters (Figure S4I). These data strongly suggest that Mfn2 is directly responsible for the liver abnormalities found in L-KO mice.

Normalization of ER stress triggered by Mfn2 deficiency ameliorates inflammation and fibrosis but not the impaired lipid metabolism

The up-regulation of UPR proteins, such as CHOP, is sufficient to promote liver apoptosis, inflammation, compensatory proliferation, fibrosis and liver cancer[48]. To begin to elucidate the mechanisms by which Mfn2 deficiency triggers the development of cancer, we examined the contribution of ER stress to these processes in the L-KO model. We blocked ER stress by overexpressing a critical regulator of UPR signaling, BIP (GRP-78). Because hepatic BIP gain-of-function in control mice has been shown to cause hypoglycemia and sudden death, even upon administration of very low levels of adenovirus, in models that do not present UPR activation (data not shown and previous reports[49,50]), we expressed BIP by adenoviral intravenous injection only in L-KO mice, which show chronic ER stress.

Acute BIP overexpression decreased UPR signaling in L-KO mice (Figure 2A, and S5A). Moreover, liver and plasma circulating pro-inflammatory cytokines were normalized by BIP (Figure 2B, and 2C), and the expression of genes encoding pro-inflammatory or fibrotic factors was also markedly lower than that seen in equivalent controls (Figure 2D and S5B). Similarly, apoptosis and cell proliferation were decreased in L-KO mice expressing BIP (Figure S5C–D). In the context of mitochondrial metabolism, BIP expression enhanced oleate oxidation (Figure S5E) and reduced ROS production measured as hydrogen peroxide (Figure S5F), thereby recovering mitochondrial function, which is in keeping with our previous data[29]. Intriguingly, BIP overexpression failed to restore hepatic triglyceride levels (Figure 2E) or the incorporation of oleate into lipids (Figure 2F). These data indicate that the hepatic mitochondrial dysfunction, inflammation, fibrosis, apoptosis and increased proliferation detected in L-KO mice lies downstream of ER stress and UPR signaling.

Mfn2 plays a crucial role in hepatic phospholipid metabolism

It has been reported that an aberrant phospholipid composition of the ER membrane is a potent activator of the UPR[51-53]. Accordingly, we studied the total hepatic phospholipid content in L-KO mice in an attempt to identify mechanisms linking Mfn2 deficiency and UPR. Results from lipidomics analysis showed that L-KO mice had a decreased abundance of total hepatic PE and PC species (Figure 3A; statistical significance of the data is shown in Supplementary Table 2). Consistent with these data, the lipidomics profile of hepatic MAMs and mitochondrial fractions from L-KO and control mice was different (Figures S6A, and S6D), with a decrease in the abundance of PE and PC species in the former (Figures S6B, S6C, S6E, and SEF; Supplementary Table 3). Because Mfn2 and some proteins of hepatic phospholipid synthesis are localized in mitochondria-ER contact sites (schematic shown in Figure 3B)[26,29,54,55], we monitored the incorporation of radiolabeled L-serine (L-Ser) into PS, PE, and PC in hepatic MAM fractions from control and L-KO mice. We found that this incorporation was significantly decreased in MAM fractions from L-KO mice (Figure 3C–E).

We next questioned whether ER stress plays a role in the defects detected in phospholipid synthesis by analyzing BIP-expressing L-KO mice. BIP expression failed to improve the incorporation of L-Ser into PS, PE or PC (Figure 3F); however, re-expression of Mfn2 completely rescued L-Ser incorporation into phospholipids (Figure 3G). Overall, our data indicate that hepatic Mfn2 depletion alters phospholipid synthesis and that these effects are not a consequence of ER stress.

Phospholipid metabolism in mammalian cells depends on the activity of many enzymes including phosphatidylserine synthase 1 (PSS1), phosphatidylserine synthase 2 (PSS2), and PE N-methyltransferase (PEMT), which are localized in MAMs and the ER; and PS decarboxylase (PISD), which is found in mitochondria[20,21]. We therefore analyzed whether loss of Mfn2 altered the expression of these proteins. Analysis by western blotting showed that the hepatic expression of PSS1 and PSS2 proteins was significantly lower in L-KO mice than in control mice (Figure 3H), whereas no changes were observed for PEMT (Figure S6G) or PISD (data not shown).

We next assessed the protein composition in MAMs by examining the abundance of MAM-enriched proteins in liver upon subcellular fractionation (Figure 3I and S6H). Western blotting of hepatic MAM fractions revealed a 50% reduction in PSS1 expression in L-KO mice (Figure 3I), whereas no changes were found for PSS2 whose expression was barely detectable (Figure 3I, and Figure S6I). Moreover, levels of PACS-2, Sig1R, and calnexin were elevated in MAMs from L-KO mice (Figures 3I, S6H, and S6I), which resembles the alterations in MAM composition in models of insulin resistance and aberrant lipid metabolism[52,56]. Thus, our results suggest that Mfn2 regulates phospholipid biosynthesis through PSS1 and PSS2 protein levels.

Alterations of lipid metabolism in L-KO mice are independent of the distance between ER and mitochondria

Given the role of Mfn2 in tethering ER to mitochondria [26-28], we explored whether the distance between mitochondria and ER might regulate phospholipid synthesis in Mfn2-ablated conditions. To do this, we used a recombinant adenovirus construct encoding a synthetic linker (RFP-linker) that increases the number ER-mitochondria contact sites, thus forcing ER-mitochondria interactions in L-KO mice (Figure S7A). Western blot analysis of RFP expression confirmed the expression of the linker (Figure S7A). L-KO mice expressing this linker showed a normalization of L-Ser incorporation into PS (Figure S7B); however, it failed to correct the synthesis of PE or PC, hepatic triacylglyceride levels, ER stress or PSS1 expression (Figures S7B–S7F). Under these conditions, PSS2 abundance was actually enhanced in L-KO mice (Figure S7F), which may explain the normalization of PS synthesis (Figure S7B). These results indicate that altered ER-mitochondria contact does not explain the lower synthesis of PE and PC in MAMs of Mfn2-deficient livers.

Down-regulation of hepatic PSS1/2 phenocopies Mfn2 ablation

In light of the above findings, we hypothesized that a decrease in phospholipid synthesis in MAMs causes hepatic triglyceride accumulation and ER stress in liver. To test this, we induced downregulation of either PSS1 or PSS2 in wild-type mice. Silencing of PSS1 by intravenous injection of a specific shRNA adenovirus caused the upregulation

of hepatic PSS2 and *vice versa* (Figure S8A,B), observations that are in agreement with previous data[57-61]. On the basis of these findings, which point to a strong adaptation process, we silenced both PSS1 and PSS2 in wild-type mice using two specific shRNA adenoviruses, which decreased the hepatic expression of both proteins by ~90% (Figure 4A and S8C). Analysis of hepatic MAM fractions showed a significant decrease of PSS1 in PSS1/2 knockdown (hereafter termed KD) mice (Figure 4B). This resulted in a decrease in the incorporation of L-Ser into PS and PE (Figure 4C) and an increase in hepatic triacylglycerol and oleate incorporation into lipids (Figure 4D and S8D). KD mice also showed ER stress (Figure 4E and S8E), and a higher expression of the fibrosis gene α-SMA and pro-inflammatory genes in liver (Figure 4F and S8F). In keeping with these observations, levels of hepatic pro-inflammatory cytokines were elevated in KD livers (Figure S8G); however, mitochondrial function (oleate oxidation or liver hydrogen peroxide production) was unaltered (Figure S8H and S8I).

Analysis of MAM protein composition revealed alterations in response to hepatic PSS1/2 silencing, with a significant decrease of Mfn2 expression in KD mice (Figure 4G). Also, PACS-2, Sig1R, and calnexin proteins were more abundant in MAMs from KD mice (Figures S8J–S8L), thus mirroring the alterations in MAM composition in Mfn2 L-KO mice. Overall, these results indicate that hepatic PSS1/2 deficiency recapitulates many of the hepatic alterations caused by Mfn2 ablation.

We next attempted to counter the liver alterations in L-KO mice by overexpressing PSS1 (Figure 4H). PSS1 overexpression led to an upregulation of Ptdss2 mRNA in L-KO mice (Figure 4I). As expected, we also found an increase in the synthesis of PS (Figure 4J), and surprisingly the normalization of liver triglycerides (Figure 4K). By contrast, PSS1 overexpression failed to rescue the synthesis of PE or PC (Figure 4J), or ameliorate the UPR (Figure 4L and S8M). Taken together, our data show that Mfn2 depletion causes a fundamental defect that prevents the synthesis of PE from PS.

Mfn2 is a PS-binding protein and generates PS-rich domains in membranes

A key process in the synthesis of phospholipids in MAMs is the transfer of PS and PE between the ER and mitochondria[20,22,25]. To determine whether Mfn2 was involved in PS transfer, we first investigated whether it binds phospholipids by assaying binding of

immunoprecipitated Mfn2 to lipid strips. Mfn2 was specifically immunoprecipitated under denaturing immunoprecipitation conditions with a polyclonal antibody. Mfn2 specifically bound phosphatidate (PA) and PS but not phosphatidylinositol (PI), PE or PC (Figure 5A). To validate this binding to phospholipids and to exclude the possibility that it was due to transmembrane domains, we constructed a truncated version of Mfn2 lacking the transmembrane domains and the C-terminal cytosolic portion (1–613), but preserving some metabolic characteristics of the full-length protein[62]. L-KO mice were tail vein injected with an adenoviral vector permitting the hepatic expression of this short form containing a 6×His tag at the N-terminus. We then purified the recombinant Mfn2 protein under denaturing conditions by affinity chromatography. Results showed that Mfn2 (1–613) could also specifically bind PS and PA (Figures 5B). To determine its potential *in vivo* role on phospholipid synthesis, we analyzed the effects on phospholipid synthesis by monitoring the incorporation of labeled L-Ser in the same L-KO mice. Data revealed that Mfn2 (1–613) enhanced the incorporation of L-Ser into PS, PE and PC (Figure 5C).

For *in vitro* analysis, we expressed Mfn2 (1–613) in *E. coli* and purified the protein by affinity chromatography that, after elution, represented >60% of the Comassie blue-stained proteins in gel electrophoresis (Figure 5D). Eluted Mfn2 (1–613) was also identified by mass spectrometry and contaminants were detected at very low levels (Supplementary Table 4). When we analyzed the capacity of the recombinant protein to bind phospholipids, we observed specific binding to PS and to PA in lipid strip assays (Figures 5E), consistent with the results in the liver. To exclude false positive binding due to phospholipid positioning in the strip, we performed liposome flotation assays, which confirmed that Mfn2 (1–613) mainly bound PS conjugated to a fluorophore (NBD) and also natural PS (Figures 5F and S9A) in liposomes. Overall, these data indicate that Mfn2 shows a capacity to selectively bind PS with minimal binding to natural PA and PI.

We next determined whether Mfn2 participates in the transfer of PS between membranes. We first evaluated its capacity to extract PS from liposomes, which may account for the alterations in the synthesis of PE in L-KO liver, even upon PSS1 overexpression. Phospholipid extraction was performed as described by Kawano et al[63]. Purified Mfn2 (1–613) was incubated with liposomes containing labeled phospholipids

(NBD-PS or NBD-PE) and the mixture was then separated by gradient centrifugation (Figure 5G). Subsequently, we analyzed the liposome-containing fraction and the non-liposome-containing fraction. Analysis of the distribution of NBD fluorescence in the presence of Mfn2 revealed that the fluorescence of NBD-PS decreased in the liposome fraction and increased in the non-liposome fraction (Figure 5H), whereas the distribution of NBD-PE fluorescence was unchanged both in the presence or absence of Mfn2 (Figure S9B).

In accord with these data, confocal microscopy revealed that Mfn2 (1–613) induced the formation of rigid domains containing exclusively NBD-PS (green color) from liposomes containing both NBD-PS (green) and Rhodamine-PE (red) (Figure 5I). Lipid domains were not generated when Mfn2 (1–613) was exposed to liposomes containing NBD-PC and Rhodamine-PE (Figure S9C). Given the unexpected capacity of Mfn2 (1–613) to generate PS-rich domains in membranes, we evaluated whether this capacity showed time-dependence and if it occurred with different types of liposomes. Using a well-established fluorescence resonance energy transfer-based membrane assay[64,65], we incubated control and Mfn2 (1–613) proteins with a mix of donor liposomes (containing NBD-phospholipids and Rhodamine-PE) and acceptor liposomes (non-fluorescent). The presence of Mfn2 (1–613) induced the release of NBD fluorescence in a time-dependent manner in liposomes containing NBD-PS but not NBD-PE (Figures 5J and S9D). Similar results were obtained using liposomes containing fluorescent TopFluor (TopFluor-PS or TopFluor-PE) derivatives of phospholipids, which are smaller in size than NBD-phospholipids (Figures S9E, and S9F). Our results support the view that Mfn2 binds PS and has the capacity to isolate it from membranes and to form rigid domains enriched in PS. These findings are consistent with a role for Mfn2 in exchanging lipids from different membranes or remodeling them in membranes, which may be due to lipid rearrangement.

PS-dependent remodeling activity of Mfn2 requires an intact N-terminal region

To address the specificity of Mfn2 functions, we tested whether Mfn1 has the same activities. To evaluate similar protein fragments in Mfn1 and in Mfn2, we expressed a recombinant truncated version of Mfn1 (1–592) in *E. coli*, which was purified under identical conditions as for Mfn2 (1–613) (Figure 6A). We first determined whether

Mfn1 (1–592) had phospholipid-binding activity. Liposome flotation assays revealed that, in contrast to Mfn2 (1–613), Mfn1 bound PC, PE, and PS phospholipids to a similar extent (Figure 6B). In a second analysis, lipid extraction assays revealed that Mfn1(1–592) failed to extract NBD-PS from liposomes (Figure 6C), but it did extract NBD-PE (Figure 6D), pointing to distinct functions for Mfn1 and Mfn2.

To better understand the basis for the differential capacity of Mfn1 and Mfn2 to bind and extract phospholipids, we examined the amino acid sequences of the two proteins (Figure 6E). Alignment analysis revealed that the N-terminal (20 aa residues) sequence of Mfn2 was absent in Mfn1. We then expressed and purified a mutant form of Mfn2 lacking this fragment (referred to as Mfn2 21–613) in *E.coli* (Figure 6F) and used it in liposome flotation assays. Results showed that Mfn2 (21–613) bound to PS, PE, PC (Figure 6G). Notably, lipid extraction assays revealed that purified Mfn2 (21–613) extracted both NBD-PS and NBD-PE from liposomes (Figure 6H and 6I). Thus, the Mfn2 (21–613) mutant combines the properties of both Mfn1 and Mfn2, suggesting that the N-terminal fragment is key to confer selectivity to extract PS.

Re-expression of Mfn2 in mice on MCD diet alleviates liver disease

After establishing the unique action of Mfn2 on phospholipid partition and metabolism, we next examined the consequences in liver under conditions of reduced Mfn2 expression during NASH. Specifically, we assessed whether the reduced Mfn2 levels in mice on MCD diet was linked to impaired PS transfer and whether it was key to the pathological alterations. We also investigated the possible role of ER stress in this scenario. Mice were placed on MCD or chow diet for two weeks and were then intravenously injected with a control adenovirus or with adenoviruses encoding Mfn2 or BIP, and livers were studied one week later. Hepatic Mfn2 expression was normalized in MCD mice upon injection of Mfn2 adenoviruses (Figures S10A, and S10C), whereas BIP failed to recover Mfn2 levels (Figures S10B and S10C). Compared with the control diet, the MCD diet induced an enhanced incorporation of radiolabeled L-Ser into PS, and a low synthesis of PE and PC in hepatic MAMs (Figure 7A). Mfn2 re-expression normalized the incorporation of L-Ser into PE and PC, whereas BIP did not ameliorate as Mfn2 the low levels of phospholipid synthesis (Figure 7A).

Analysis of fibrosis in liver sections of MCD diet-fed mice showed that Mfn2-re-expressing mice had less Sirius red staining than mice treated with control adenovirus (Figure 7B), whereas the expression of BIP only partially diminished fibrosis (Figure 7B). Similarly, triglyceride accumulation in liver was decreased upon Mfn2 re-expression as assessed by H&E staining (Figure 7B), and by quantification of triglycerides (Figure 7C). By contrast, BIP expression failed to normalize hepatic triglycerides in MCD diet-fed mice (Figure 7B, and 7C). As expected, the expression of inflammatory and fibrosis markers was markedly decreased by Mfn2 re-expression, but not by BIP overexpression (Figures 7D). Finally, both BIP and Mfn2 treatments normalized all UPR markers upregulated in MCD mice (Figure S10D).

Overall, our data strongly suggest that Mfn2 repression plays a key role in the development of steatosis, inflammation and fibrosis in a mouse model of NASH. Moreover, we have identified a defect in phospholipid synthesis in MCD diet-fed mice, which it is crucial for the development of the pathology. Our data are consistent with a major role of Mfn2 in the normalization of PS transfer from ER to mitochondria, which seems critical for the amelioration of liver disease.

Discussion

We report that Mfn2 plays a key role in liver homeostasis by controlling both PS transfer from ER to mitochondria and the UPR. Accordingly, hepatic ablation of Mfn2 results in unbalanced phospholipid metabolism, leading to ER stress and triggering liver inflammation and fibrosis, which takes place early in the life of these mice and occurs even on a normal diet and in the absence of obesity. In addition, mice with liver-specific knockout of Mfn2 have enhanced susceptibility to liver cancer with age or in response to carcinogenic agents. Supporting the clinical relevance of these findings, we show that hepatic Mfn2 expression is lower in patients with NASH than in those with steatosis. Mfn2 expression is also repressed in mouse models of steatosis and NASH, and its re-expression diminishes NASH-like liver pathologies. Taken together, our data indicate that hepatic Mfn2 is a key protein to maintain healthy liver function and its repression is involved in the development of liver disease.

We show that the UPR caused by Mfn2 deficiency plays a key role in the development of hepatic inflammation, apoptosis, compensatory proliferation and fibrosis, which in turn contributes to the development of liver cancer[48]. Thus, normalization of UPR response by BIP gain-of-function restores inflammation to control levels and reduces apoptosis, hyper-proliferation and fibrosis, which would prevent the development of cancer. These results are consistent with our previous observations that deficient hepatic insulin signaling is normalized in Mfn2 knockout mice treated with tauroursodeoxycholic acid[31]. Indeed, chronic ER stress plays a key role in the pathophysiology associated with Mfn2 deficiency, and appears to be responsible for the alterations in mitochondrial metabolism that have been detected in Mfn2-deficient cells[29]. The fact that inflammation, fibrosis and insulin resistance are modulated by ER stress may explain the relationship reported between steatosis, insulin resistance, and NASH[48,52,66-68].

We found that Mfn2 re-expression normalizes liver function in a mouse model of NASH, whereas BIP expression only partially counters steatosis, inflammation and fibrosis. These findings indicate that whereas Mfn2 likely plays a key role in the

development of liver disease in murine NASH, the UPR is a secondary contributing factor.

Our data also reveal that Mfn2 deficiency markedly impairs phospholipid metabolism and this lies upstream of the UPR. Thus, BIP-induced amelioration of UPR failed to normalize lipid metabolism. The changes in phospholipid metabolism associated with Mfn2 deficiency were characterized by lower rates of synthesis of PS, PE and PC, reduced expression of phosphatidylserine synthases PSS1 and PSS2, and reduced abundance of PSS1 in MAM fractions. We also found that a reduction in hepatic phospholipid metabolism explains the enhanced accumulation of triglycerides, the UPR and inflammation. While the re-expression of PSS1 was not sufficient to mitigate the defective synthesis of PE and PC in Mfn2-depleted livers, it significantly reduced hepatic triglycerides, revealing a close regulation of phospholipid and triglyceride synthesis in MAMs. Expression of both full-length and truncated Mfn2, lacking the transmembrane domains, improved phospholipid metabolism in Mfn2-deficient livers. Thus, our results indicate that loss of hepatic Mfn2 expression changes phospholipid metabolism by altering two different steps: 1) reducing the transfer of PS from the ER to mitochondria, and 2) inhibiting PS synthesis as a consequence of a compensatory reduced expression of PPS1 and PSS2.

Importantly, we describe a new molecular function of Mfn2 in the maintenance of hepatic phospholipid metabolism. Mfn2 has the capacity to bind PS *in vitro*, and to cause partitions of PS into rigid membrane domains. These activities are specific for PS and are not found with other phospholipids such as PE or PC. Indeed, these data may be key to understand the molecular basis for the multiple cellular effects of Mfn2[26,31,32,69]. In addition, our observations provide molecular insights into the steps involved in the transfer of PS from ER to mitochondria. We propose that Mfn2 participates in the generation of PS-enriched domains at the ER-mitochondria contact sites and they favor the activity of potential PS transport proteins such as the oxysterol-binding protein (OSBP)-related proteins ORPs (ORP5/ORP8) or VAT-1. ORP5/8 binds PS in vitro[70] and mediates PI4P/PS counter transport between the ER and the plasma membrane[71]. These proteins have also been identified in MAMs[72] and therefore may participate in the transfer of PS between ER and mitochondria.

The observation of a link between Mfn2 and phospholipids is highly relevant because of their influence on membrane-dependent cellular functions, antioxidant, anti-inflammatory, anti-fibrotic properties, and cellular signaling[73,74]. Thus, obesity has been reported to increase the hepatic PC/PE ratio which inhibits SERCA activity[75]. In addition, genetic inhibition of PEMT, which catalyzes the conversion of PE to PC, relieves ER stress and improves systemic glucose homeostasis in obesity[75,76]. Mfn2 levels are increased in MAMs in obese mice[56] under conditions in which enhanced PC production has been reported[75]. Furthermore, low levels of phospholipids in bile due to the disruption of membrane transporters are linked to liver disease[77,78]. Another important feature of our work is the observation that hepatic Mfn2 ablation provokes MAM remodeling similar to that detected in HFD or genetic obesity. This is also relevant because remodeling of MAM interactions in liver in obesity has been shown to result in undesirable side effects such as triacylglycerol accumulation and insulin resistance[56]. Specifically, hepatic MAM shows an enhanced abundance of protein markers such as PACS2, IP3R1, and IP3R2 during obesity[56], which is consistent with the pattern of changes detected in Mfn2-deficient livers. Accordingly, we propose that alterations in Mfn2 expression have an impact on MAM reorganization, perhaps through changes in the phospholipid composition in ER-mitochondrial contact sites. These observations also reveal that changes to Mfn2 levels may alter the composition of tethers at ER-mitochondrial contact sites, and this may be dependent on the cell context. In addition, those data complement the observations that disruption of individual MAM components seem to be sufficient to alter phospholipid synthesis in disorders such as Alzheimer disease and Lenz-Majewski syndrome[79-81].

In contrast to the function of Mfn2, Mfn1 shows a broader phospholipid binding activity but it does not generate PE- or PC-rich domains. The N-terminal region (20 amino acid residues) of Mfn2 (not present in Mfn1) is key for PS specificity, as elimination of this region generates a mutant form of Mfn2 incorporating the capacities of Mfn1 and Mfn2, indicating a hybrid behavior. Further studies will be needed to understand the molecular basis for the PS binding and extraction activities of Mfn2.

In conclusion, our data support the view that Mfn2 sustains PS transfer to the mitochondria for conversion to PE. The effects on phospholipid metabolism may explain the role of Mfn2 in the maintenance of MAMs and proper lipid metabolism and

ER homeostasis. Thus, we propose Mfn2 as a potential therapeutic target for counteracting the development of liver disease related to NASH and liver cancer.

Experimental Procedures.

Experimental Procedures see Supplemental Information.

Author contributions

M.I.H.-A. conceived, designed the study and the strategy, performed experiments, discussed the results and wrote the manuscript; D. Sebastián, S.V., P.B., P.K., N.P., S.R.V., V.H., N.V., P.G., A.A., M.J.,R.P., I.G., E.C.,N.C., R.C., A.K., M.B., D.S., T.H., J.F., E.E-M, M.O., J.J., performed experiments; S.I. conceived and performed experiments; A.B-L performed the total liver lipidomics statistical analysis; M.O, C.C. M.P., S.F-V and J.V. revised experimental data and contributed to the discussion. A.Z. designed the study and the strategy, discussed the results, and wrote the manuscript.

Acknowledgements.

We thank Dr. Jennifer Rieusset for the BIP adenovirus and Dr. Estela Area-Gomez for sharing with us the protocol of phospholipid synthesis. We also thank the Unit of Electron Cryo-Microscopy (Scientific and Technological Centers, *Universitat de Barcelona*), Dr. Mar García-Rocha for discussion and Jorge Manuel Seco for technological assistance. We thank Dr. Helena Cortez-Pinto (Department of Gastroenterology, Hospital Santa Maria, Lisbon, Portugal) for providing the liver biopsies. We thank Neus Prats and the histopathology facility for the pathologic analysis of the mouse samples. We thank also the protein expression core facility for the production of short form Mfn2 in *E. coli*. M.I. Hernández-Alvarez was the recipient of a predoctoral fellowship from the CONACYT, Mexico, and is recipient of a postdoctoral fellowship "Juan de la Cierva Incorporación". This study was supported by research grants from the MINECO (SAF2016-75246R), Grant 2014SGR48 from the *Generalitat de Catalunya*, INFLAMES (PIE-14/00045) from the Instituto de Salud Carlos III, CIBERDEM ("Instituto de Salud Carlos III"), and INTERREG IV-B-SUDOE-FEDER (DIOMED, SOE1/P1/E178). A.Z. is a recipient of an ICREA "Academia" (*Generalitat*

de Catalunya). We gratefully acknowledge institutional funding from the MINECO through the Centres of Excellence Severo Ochoa Award, and from the CERCA Program of the Generalitat de Catalunya.

References.

1. Chalasani, N.*, et al.* The diagnosis and management of non-alcoholic fatty liver disease: practice Guideline by the American Association for the Study of Liver Diseases, American College of Gastroenterology, and the American Gastroenterological Association. *Hepatology* **55**, 2005-2023 (2012).
2. Yeh, M.M. & Brunt, E.M. Pathological features of fatty liver disease. *Gastroenterology* **147**, 754-764 (2014).
3. Brenner, C., Galluzzi, L., Kepp, O. & Kroemer, G. Decoding cell death signals in liver inflammation. *Journal of Hepatology* **59**, 583-594 (2013).
4. Aravalli, R.N., Steer, C.J. & Cressman, E.N. Molecular mechanisms of hepatocellular carcinoma. *Hepatology* **48**, 2047-2063 (2008).
5. Aravalli, R.N., Cressman, E.N. & Steer, C.J. Cellular and molecular mechanisms of hepatocellular carcinoma: an update. *Arch Toxicol* **87**, 227-247 (2013).
6. Demaria, S.*, et al.* Cancer and inflammation: promise for biologic therapy. *J Immunother* **33**, 335-351 (2010).
7. Mantovani, A., Allavena, P., Sica, A. & Balkwill, F. Cancer-related inflammation. *Nature* **454**, 436-444 (2008).
8. Grivennikov, S.I., Greten, F.R. & Karin, M. Immunity, inflammation, and cancer. *Cell* **140**, 883-899 (2010).
9. Coussens, L.M. & Werb, Z. Inflammation and cancer. *Nature* **420**, 860-867 (2002).
10. Tilg, H. & Hotamisligil, G.S. Nonalcoholic fatty liver disease: Cytokine-adipokine interplay and regulation of insulin resistance. *Gastroenterology* **131**, 934-945 (2006).
11. Dumas, M.E.*, et al.* Metabolic profiling reveals a contribution of gut microbiota to fatty liver phenotype in insulin-resistant mice. *Proceedings of the National Academy of Sciences of the United States of America* **103**, 12511-12516 (2006).
12. Miele, L.*, et al.* Increased intestinal permeability and tight junction alterations in nonalcoholic fatty liver disease. *Hepatology* **49**, 1877-1887 (2009).
13. Dara, L., Ji, C. & Kaplowitz, N. The contribution of endoplasmic reticulum stress to liver diseases. *Hepatology* **53**, 1752-1763 (2011).
14. Alkhouri, N., Dixon, L.J. & Feldstein, A.E. Lipotoxicity in nonalcoholic fatty liver disease: not all lipids are created equal. *Expert review of gastroenterology & hepatology* **3**, 445-451 (2009).
15. Begriche, K., Massart, J., Robin, M.A., Bonnet, F. & Fromenty, B. Mitochondrial adaptations and dysfunctions in nonalcoholic fatty liver disease. *Hepatology* **58**, 1497-1507 (2013).
16. Schenkel, L.C. & Bakovic, M. Formation and Regulation of Mitochondrial Membranes. *International Journal of Cell Biology* **2014**, 13 (2014).
17. Tatsuta, T., Scharwey, M. & Langer, T. Mitochondrial lipid trafficking. *Trends in Cell Biology* **24**, 44-52 (2014).
18. Ardail, D.*, et al.* Mitochondrial contact sites. Lipid composition and dynamics. *Journal of Biological Chemistry* **265**, 18797-18802 (1990).
19. Paradies, G., Paradies, V., Ruggiero, F.M. & Petrosillo, G. Oxidative stress, cardiolipin and mitochondrial dysfunction in nonalcoholic fatty liver disease. *World Journal of Gastroenterology : WJG* **20**, 14205-14218 (2014).
20. Osman, C., Voelker, D.R. & Langer, T. Making heads or tails of phospholipids in mitochondria. *The Journal of Cell Biology* **192**, 7-16 (2011).
21. Flis, V.V. & Daum, G. Lipid Transport between the Endoplasmic Reticulum and Mitochondria. *Cold Spring Harbor Perspectives in Biology* **5**(2013).
22. Raturi, A. & Simmen, T. Where the endoplasmic reticulum and the mitochondrion tie the knot: The mitochondria-associated membrane (MAM). *Biochimica et Biophysica Acta (BBA) - Molecular Cell Research* **1833**, 213-224 (2013).

23. Vance, J.E. & Vance, D.E. Phospholipid biosynthesis in mammalian cells. *Biochemistry and Cell Biology* **82**, 113-128 (2004).
24. Scharwey, M., Tatsuta, T. & Langer, T. Mitochondrial lipid transport at a glance. *Journal of Cell Science* **126**, 5317-5323 (2013).
25. Shiao, Y.J., Balcerzak, B. & Vance, J.E. A mitochondrial membrane protein is required for translocation of phosphatidylserine from mitochondria-associated membranes to mitochondria. *Biochemical Journal* **331**, 217-223 (1998).
26. de Brito, O.M. & Scorrano, L. Mitofusin 2 tethers endoplasmic reticulum to mitochondria. *Nature* **456**, 605-610 (2008).
27. Leal, N.S*., et al.* Mitofusin-2 knockdown increases ER-mitochondria contact and decreases amyloid beta-peptide production. *J Cell Mol Med* **20**, 12863 (2016).
28. Wang, L*., et al.* Mitofusin 2 Regulates Axonal Transport of Calpastatin to Prevent Neuromuscular Synaptic Elimination in Skeletal Muscles. *Cell metabolism* **28**, 400-414 e408 (2018).
29. Muñoz, J.P*., et al.* Mfn2 modulates the UPR and mitochondrial function via repression of PERK. *The EMBO journal* **32**, 2348-2361 (2013).
30. Schneeberger, M*., et al.* Mitofusin 2 in POMC neurons connects ER stress with leptin resistance and energy imbalance. *Cell* **155**, 172-187 (2013).
31. Sebastián, D*., et al.* Mitofusin 2 (Mfn2) links mitochondrial and endoplasmic reticulum function with insulin signaling and is essential for normal glucose homeostasis. *Proceedings of the National Academy of Sciences* **109**, 5523-5528 (2012).
32. Bach, D*., et al.* Mitofusin-2 Determines Mitochondrial Network Architecture and Mitochondrial Metabolism: A NOVEL REGULATORY MECHANISM ALTERED IN OBESITY. *Journal of Biological Chemistry* **278**, 17190-17197 (2003).
33. Pich, S*., et al.* The Charcot–Marie–Tooth type 2A gene product, Mfn2, up-regulates fuel oxidation through expression of OXPHOS system. *Human Molecular Genetics* **14**, 1405-1415 (2005).
34. Rehman, J*., et al.* Inhibition of mitochondrial fission prevents cell cycle progression in lung cancer. *Faseb J* **26**, 2175-2186 (2012).
35. Wang, W*., et al.* Pro-apoptotic and anti-proliferative effects of mitofusin-2 via Bax signaling in hepatocellular carcinoma cells. *Med Oncol* **29**, 70-76 (2012).
36. Xu, K*., et al.* MFN2 suppresses cancer progression through inhibition of mTORC2/Akt signaling. *Sci Rep* **7**(2017).
37. Cheng, X., Zhou, D., Wei, J. & Lin, J. Cell-cycle arrest at G2/M and proliferation inhibition by adenovirus-expressed mitofusin-2 gene in human colorectal cancer cell lines. *Neoplasma* **60**, 620-626 (2013).
38. Wu, Y*., et al.* Clinical significance of mitofusin-2 and its signaling pathways in hepatocellular carcinoma. *World J Surg Oncol* **14**, 016-0922 (2016).
39. Zhou, X*., et al.* MicroRNA-761 is upregulated in hepatocellular carcinoma and regulates tumorigenesis by targeting Mitofusin-2. *Cancer Sci* **107**, 424-432 (2016).
40. Qu, L., Chen, H., Wang, G. & Wei, J. Frequent losses of heterozygosity in the mitofusin 2 gene in hepatocellular carcinoma: their relationship to clinicopathological features. *Tumori* **99**, 697-701 (2013).
41. Ferreira, D.M.S*., et al.* Apoptosis and insulin resistance in liver and peripheral tissues of morbidly obese patients is associated with different stages of non-alcoholic fatty liver disease. *Diabetologia* **54**, 1788-1798 (2011).
42. Takeda, D*., et al.* Effect of preoperative chemotherapy on postoperative liver regeneration following hepatic resection as estimated by liver volume. *World J Surg Oncol* **11**, 1477-7819 (2013).
43. Gaemers, I.C*., et al.* Lipotoxicity and steatohepatitis in an overfed mouse model for non-alcoholic fatty liver disease. *Biochimica et Biophysica Acta (BBA) - Molecular Basis of Disease* **1812**, 447-458 (2011).

44. Matsumoto, M.*, et al.* An improved mouse model that rapidly develops fibrosis in non-alcoholic steatohepatitis. *International Journal of Experimental Pathology* **94**, 93-103 (2013).
45. Malhi, H., Guicciardi, M.E. & Gores, G.J. Hepatocyte death: a clear and present danger. *Physiological reviews* **90**, 1165-1194 (2010).
46. Sun, B. & Karin, M. Obesity, inflammation, and liver cancer. *J Hepatol* **56**, 704-713 (2012).
47. Herranz, D.*, et al.* Sirt1 improves healthy ageing and protects from metabolic syndrome-associated cancer. *Nat Commun* **1**, 3 (2010).
48. DeZwaan-McCabe, D.*, et al.* The Stress-Regulated Transcription Factor CHOP Promotes Hepatic Inflammatory Gene Expression, Fibrosis, and Oncogenesis. *PLoS Genet* **9**, e1003937 (2013).
49. Sch, #xf6 & nthal, A.H. Endoplasmic Reticulum Stress: Its Role in Disease and Novel Prospects for Therapy. *Scientifica* **2012**, 26 (2012).
50. Lee, A.S. The glucose-regulated proteins: stress induction and clinical applications. *Trends in Biochemical Sciences* **26**, 504-510 (2001).
51. Fagone, P. & Jackowski, S. Membrane phospholipid synthesis and endoplasmic reticulum function. *Journal of Lipid Research* **50**, S311-S316 (2009).
52. Fu, S.*, et al.* Aberrant lipid metabolism disrupts calcium homeostasis causing liver endoplasmic reticulum stress in obesity. *Nature* **473**, 528-531 (2011).
53. Halbleib, K.*, et al.* Activation of the Unfolded Protein Response by Lipid Bilayer Stress. *Molecular Cell* **67**, 673-684.e678.
54. Singaravelu, K.*, et al.* Mitofusin 2 regulates STIM1 migration from the Ca2+ store to the plasma membrane in cells with depolarized mitochondria. *The Journal of biological chemistry* **286**, 12189-12201 (2011).
55. Stone, S.J. & Vance, J.E. Phosphatidylserine Synthase-1 and -2 Are Localized to Mitochondria-associated Membranes. *Journal of Biological Chemistry* **275**, 34534-34540 (2000).
56. Arruda, A.P.*, et al.* Chronic enrichment of hepatic endoplasmic reticulum-mitochondria contact leads to mitochondrial dysfunction in obesity. *Nat Med* **20**, 1427-1435 (2014).
57. Steenbergen, R., Nanowski, T.S., Nelson, R., Young, S.G. & Vance, J.E. Phospholipid homeostasis in phosphatidylserine synthase-2-deficient mice. *Biochimica et Biophysica Acta (BBA) - Molecular and Cell Biology of Lipids* **1761**, 313-323 (2006).
58. STONE, S.J. & VANCE, J.E. Cloning and expression of murine liver phosphatidylserine synthase (PSS)-2: differential regulation of phospholipid metabolism by PSS1 and PSS2. *Biochemical Journal* **342**, 57-64 (1999).
59. Vance, J.E. & Tasseva, G. Formation and function of phosphatidylserine and phosphatidylethanolamine in mammalian cells. *Biochimica et Biophysica Acta (BBA) - Molecular and Cell Biology of Lipids* **1831**, 543-554 (2013).
60. Bergo, M.O.*, et al.* Defining the Importance of Phosphatidylserine Synthase 2 in Mice. *Journal of Biological Chemistry* **277**, 47701-47708 (2002).
61. Arikketh, D., Nelson, R. & Vance, J.E. Defining the Importance of Phosphatidylserine Synthase-1 (PSS1): Unexpected Viability of PSS1-Deficient Mice. *Journal of Biological Chemistry* **283**, 12888-12897 (2008).
62. Segales, J.*, et al.* A form of mitofusin 2 (Mfn2) lacking the transmembrane domains and the COOH-terminal end stimulates metabolism in muscle and liver cells. *Am J Physiol Endocrinol Metab* **305**, 13 (2013).
63. Kawano, S.*, et al.* Structure-function insights into direct lipid transfer between membranes by Mmm1-Mdm12 of ERMES. *J Cell Biol* **217**, 959-974 (2018).
64. Connerth, M.*, et al.* Intramitochondrial Transport of Phosphatidic Acid in Yeast by a Lipid Transfer Protein. *Science* **338**, 815-818 (2012).

65. Potting, C*., et al.* TRIAP1/PRELI complexes prevent apoptosis by mediating intramitochondrial transport of phosphatidic acid. *Cell metabolism* **18**, 287-295 (2013).
66. Longato, L*., et al.* Insulin Resistance, Ceramide Accumulation, and Endoplasmic Reticulum Stress in Human Chronic Alcohol-Related Liver Disease. *Oxidative Medicine and Cellular Longevity* **2012**, 17 (2012).
67. Tilg, H. & Moschen, A.R. Evolution of inflammation in nonalcoholic fatty liver disease: The multiple parallel hits hypothesis. *Hepatology* **52**, 1836-1846 (2010).
68. Pagliassotti, M.J. Endoplasmic Reticulum Stress in Nonalcoholic Fatty Liver Disease. *Annual Review of Nutrition* **32**, 17-33 (2012).
69. Koshiba, T*., et al.* Structural basis of mitochondrial tethering by mitofusin complexes. *Science* **305**, 858-862 (2004).
70. Maeda, K*., et al.* Interactome map uncovers phosphatidylserine transport by oxysterol-binding proteins. *Nature* **501**, 257-261 (2013).
71. Chung, J*., et al.* INTRACELLULAR TRANSPORT. PI4P/phosphatidylserine countertransport at ORP5- and ORP8-mediated ER-plasma membrane contacts. *Science* **349**, 428-432 (2015).
72. Galmes, R*., et al.* ORP5/ORP8 localize to endoplasmic reticulum-mitochondria contacts and are involved in mitochondrial function. *EMBO Rep* **17**, 800-810 (2016).
73. Gundermann, K.J., Kuenker, A., Kuntz, E. & Drozdzik, M. Activity of essential phospholipids (EPL) from soybean in liver diseases. *Pharmacol Rep* **63**, 643-659 (2011).
74. Chakravarthy, M.V*., et al.* Identification of a physiologically relevant endogenous ligand for PPARalpha in liver. *Cell* **138**, 476-488 (2009).
75. Fu, S*., et al.* Aberrant lipid metabolism disrupts calcium homeostasis causing liver endoplasmic reticulum stress in obesity. *Nature* **473**, 528-531 (2011).
76. Jacobs, R.L*., et al.* Impaired de novo choline synthesis explains why phosphatidylethanolamine N-methyltransferase-deficient mice are protected from diet-induced obesity. *The Journal of biological chemistry* **285**, 22403-22413 (2010).
77. Tanaka, N., Matsubara, T., Krausz, K.W., Patterson, A.D. & Gonzalez, F.J. Disruption of phospholipid and bile acid homeostasis in mice with nonalcoholic steatohepatitis. *Hepatology* **56**, 118-129 (2012).
78. Tarling, E.J., de Aguiar Vallim, T.Q. & Edwards, P.A. Role of ABC transporters in lipid transport and human disease. *Trends in endocrinology and metabolism: TEM* **24**, 342-350 (2013).
79. Area-Gomez, E*., et al. Upregulated function of mitochondria-associated ER membranes in Alzheimer disease*, (2012).
80. Area-Gomez, E. & Schon, E.A. Mitochondrial Genetics and Disease. *Journal of Child Neurology* **29**, 1208-1215 (2014).
81. Sousa, S.B*., et al.* Gain-of-function mutations in the phosphatidylserine synthase 1 (PTDSS1) gene cause Lenz-Majewski syndrome. *Nat Genet* **46**, 70-76 (2014).

FIGURE LEGENDS.

FIGURE 1. Mfn2 is reduced in NASH and liver-specific Mfn2 ablation in mice causes a NASH-like phenotype. A) Quantification of Mfn2 protein in liver biopsies from steatotic (NAS ≤3, n=7) and NASH (NAS ≥5, n=8) patients. B) Quantification of Mfn2 protein in liver from mice on chow diet (C) or high-fat diet (HFD) as a model of steatosis (n=4 mice per group). C) Representative H&E and Sirius red staining images in liver sections from 8-week-old C57Bl6/J mice fed either a chow diet (C) or a methionine/choline-deficient diet combined with HFD and supplemented with 0.1% L-methionine in drinking water (MCD) (scale bar, 200 μm). D) Triglyceride (TAG) levels in liver from mice on C and MCD diets (n=5 mice per group). E) Quantification of Mfn2 protein in liver from C (n=5) and MCD mice (n=4). F) Hepatic pro-inflammatory factors in control (C) and liver-specific Mfn2 KO (L-KO) mice measured by ELISA (n=8 mice per group). G) Hepatic TAG levels in C and L-KO mice (n=8–12 mice per group). H) Oleate incorporation into different lipid species in hepatocytes isolated from C and L-KO mice (n=4 mice per group, each experiment performed in triplicate). I) Representative Sirius red staining and TEM images in liver sections from 27-week-old C and L-KO mice fed a normal diet (scale bars, 200 μm in Sirius Red staining images, and 5 μm in TEM images). J) Hepatic expression of genes involved in collagen synthesis in C and L-KO mice (n=5 mice per group). K) Representative macroscopic images of liver from 24 month-old C and L-KO mice fed a normal diet, and quantification of liver tumors expressed as the mean of number of tumours in livers from 5 mice. In panel A, data are expressed as mean ± SD, and in the remaining panels as mean ± SE. *$p<0.05$ vs. control group in each case.

FIGURE 2. Normalization of ER stress ameliorates inflammation and fibrosis but not lipid metabolism in L-KO mice. Control (C) mice were studied 5 days after tail vein injection of control LacZ adenoviruses (C+AdC) and L-KO mice were studied 5 days after tail vein injection of control (LacZ) (L-KO+AdC, red bars) or BIP adenoviruses (L-KO+AdBIP, yellow bars) (n=4 mice per group). Data are expressed as values relative to control LacZ group (shown as a discontinuous line). A) Representative western blot of protein expression of hepatic ER stress markers. B)

Hepatic pro-inflammatory factors measured by ELISA. C) Plasma levels of IL-1β. D) Expression of genes involved in collagen synthesis. E) Hepatic TAG levels . F) Oleate incorporation into lipid species in isolated hepatocytes. Data are expressed as mean ± SE. Statistical analysis was performed by using one-way ANOVA followed by post-hoc t tests. *$p<0.05$ L-KO vs. C mice, $^{\$}p<0.05$ L-KO+AdBIP vs. L-KO+AdC mice.

FIGURE 3. Mfn2 ablation alters hepatic phospholipid metabolism independently of ER stress. A) Hepatic phosphatidylcholine (PC) and phosphatidylethanolamine (PE) content measured by lipidomics in control (C) (n=11) and L-KO (n=13) mice. Data are expressed as fold-change vs. C mice. Significant compounds are shown in the heatmap ($p<0.05$) out of 128 phospholipids analyzed. B) Graphical scheme of phosphatidylserine (PS), phosphatidylethanolamine (PE) and PS synthesis in mitochondria-associated ER membranes (MAMs). C–E) ^{3}H- L-serine incorporation into PS (C), PE (D), and phosphatidylcholine (PC) (E) in hepatic mitochondria-associated ER-enriched fractions from C and L-KO mice (n=5–7 mice per group). F) ^{3}H- L-serine incorporation into PS, PE and PC in hepatic mitochondria-associated ER-enriched fractions from control (lacZ injected, C+AdC), L-KO (lacZ injected, L-KO+AdC, red bars), and L-KO (BIP injected, L-KO+BIP mice, yellow bars) (n=4 mice per group). Data are expressed as values relative to C+AdC group (shown as a discontinuous line). G) ^{3}H-L-serine incorporation into PS, PE and PC in hepatic mitochondria-associated ER-enriched fractions from C+AdC, L-KO+AdC (red bars), and L-KO (Mfn2 injected, L-KO+AdMfn2 mice, grey bars) (n=4 mice per group). Data are expressed as values relative to C+AdC group (shown as a discontinuous line). H) Representative western blot showing hepatic expression of PSS1, PSS2 and PEMT proteins levels in 8-week-old C and L-KO mice (n=4 mice per group). I) Protein expression of MAM proteins in liver from C and L-KO mice (n=4 mice per group). Data are expressed as mean ± SE. Statistical analysis was performed by using one-way ANOVA followed by post-hoc t tests. *$p<0.05$ L–KO vs. C mice, $^{\$}p<0.05$ vs. L-KO+AdC mice.

FIGURE 4. Deficiency of hepatic phosphatidylserine synthase 1 and 2 phenocopies Mfn2 ablation. A) Quantification of hepatic protein expression of PSS1 and PSS2 5 days after tail vein injection with control LacZ (C) or Ptdss1/Ptdss2 (KD) siRNA

adenoviruses (n=5 mice per group). B) Quantification of PSS1 protein in MAM fractions obtained from C or KD mice (n=5 mice per group). C) ^{3}H-L-serine incorporation into PS and PE in hepatic mitochondria-associated ER-enriched fractions from C or KD mice (n=4 mice per group). D) Hepatic triglyceride (TAG) levels in C and KD mice (n=4 mice per group). E) Quantification of protein expression of hepatic ER stress markers in C and KD mice (n=4 mice per group). F) Hepatic expression of genes involved in inflammation in C and KD mice (n=5 mice per group). G) Quantification of Mfn2 protein in MAM fractions from C and KD mice. H) Scheme of PSS1 overexpression in mice. I) mRNA levels of Ptdss1 and Ptdss2 from control (lacZ injected, C+AdC), L-KO (lacZ injected, L-KO+AdC, red bars), and L-KO (Ptdss1 injected, L-KO+Ptdss1, blue bars) mice (n=3–5 mice per group). J) ^{3}H-L-serine incorporation into PS, PE and PC in hepatic mitochondria-associated ER-enriched fractions from C+AdC, L-KO+AdC (red bars), and L-KO+Ptdss1 mice (blue bars) (n=3–5 mice per group). K) Hepatic TAG levels in C+AdC, L-KO+AdC (red bars), and L-KO+Ptdss1 (blue bars) mice. L) Quantification of protein expression of hepatic ER stress markers in C+AdC, L-KO+AdC (red bars), and L-KO+Ptdss1 (blue bars) mice (n=3–5 mice per group). Data are expressed as values relative to C+AdC group (shown as a discontinuous line). Data are expressed as mean ± SE. Statistical analysis was performed by using one-way ANOVA followed by post-hoc t tests. *$p<0.05$ vs. C mice, $^{\$}p<0.05$ vs. L-KO+AdC mice.

FIGURE 5. Mfn2 binds phosphatidylserine and generates phosphatidylserine-rich domains in membranes. A) Binding of Mfn2 protein immunoprecipitated from liver to different phospholipids on a Membrane Lipid Strip^{TM}. B) Binding of a truncated form of Mfn2 (1–613), expressed in liver and purified by affinity chromatography, to phospholipids on a Membrane Lipid Strip^{TM}. C) ^{3}H-L-serine incorporation into PS, PE and PC in hepatic mitochondria-associated ER-enriched fractions from mice injected with LacZ in control (C+AdC) and L-KO (L-KO+AdC, red bars) mice and with a Mfn2 (1–613) adenovirus (L-KO+Mfn2 (1–613), blue bars) (n=4 mice per group). Data are expressed as values relative to the C+AdC group (shown as a discontinuous line). D) Representative Commassie-stained gel of the purification of Mfn2 (1–613) expressed in *E. coli*. E) Binding of Mfn2 (1–613) expressed in *E. coli* to different phospholipids on a Membrane Lipid Strip^{TM}. F) Representative western blot against Mfn2 after the

liposome flotation assay with different fluorescent (NBD) phospholipids. G) Scheme of the NBD-Phospholipid liposome extraction assay. H) Quantification of NBD-PS liposome extraction assay with Mfn2 (1–613) expressed in *E. coli* (n=6). I) Confocal microscopy images of liposomes in the absence or presence of Mfn2 (1–613), showing the formation of the NBD-PS rigid domain with Mfn2 (1–613). J) Kinetic FRET assay with NBD-PS and Rhod-PE to evaluate the capacity of Mfn2 (1–613) to dequench NBD-PS fluorescence from liposomes (n=6). Data are expressed as mean ± SE. Statistical analysis in panel H: *p<0.05 vs. C $^{\$}$p<0.05 vs. L-KO+AdC. Statistical analysis in panel J was performed by using a two-way ANOVA (*p<0.0001).

FIGURE 6. Phosphatidylserine binding and extraction activities of Mfn2 require an intact N-terminal region. A) Representative Commassie-stained gel of the purification of a short form of Mfn1 (1–592) expressed in *E. coli*. B) Representative western blot against histidine showing Mfn1 protein after the liposome flotation assay with different non-fluorescent phospholipids. C) Quantification of NBD-PS liposome extraction assay with Mfn1 (1–592) expressed in *E. coli* (n=3). D) Quantification of NBD-PE extraction assay with Mfn1 (1–592) expressed in *E. coli* (n=3). E) Mfn2 and Mfn1 human sequence alignment. F) Representative Commassie-stained gel of purification of Mfn2 (21–613) expressed in *E. coli*. G) Representative western blot against histidine showing Mfn2 (21–613) protein after the liposome flotation assay with non-fluorescent phospholipids. H) Quantification of NBD-PS liposome extraction assay with Mfn2 (21–613) expressed in *E. coli* (n=3). I) Quantification of NBD-PE liposome extraction assay with Mfn2 (21–613) expressed in *E. coli* (n=3). Data are expressed as mean ± SE. *p<0.05 vs. C.

FIGURE 7. Mfn2 re-expression improves the NASH phenotype in mice. A) ^{3}H-L-serine incorporation into PS, PE and PC in hepatic mitochondria-associated ER-enriched fractions from control mice injected with AdC (null adenovirus) (C+AdC, white bars), MCD mice injected with AdC (MCD+AdC, blue bars), with AdMfn2 (MCD+AdMfn2, red bars) or with AdBIP (MCD+BIP, yellow bars) (n=4 mice per group). B) Representative H&E and Sirius red staining images in liver sections from C+AdC, MCD+AdC, MCD+Mfn2 and MCD+BIP mice (scale bar, 200 μm). C) Hepatic

triglyceride (TAG) levels in C+AdC (white bars), MCD+AdC (blue bars), MCD+Mfn2 (red bars) and MCD+BIP (yellow bars) mice (n=4 mice per group). D) Hepatic pro-inflammatory factors and genes involved in collagen synthesis in C+AdC (white bars), MCD+AdC (blue bars), MCD+Mfn2 (red bars) and MCD+BIP (yellow bars) mice (n=4 mice per group). Data are expressed as the mean ± SE. Statistical analysis was performed by using one-way ANOVA followed by post-hoc t tests. *$p<0.05$ vs. C+AdC, $^{\$}p<0.05$ vs. MCD+AdC and $^{\#}p<0.05$ vs. MCD+AdBIP.

Figure 1

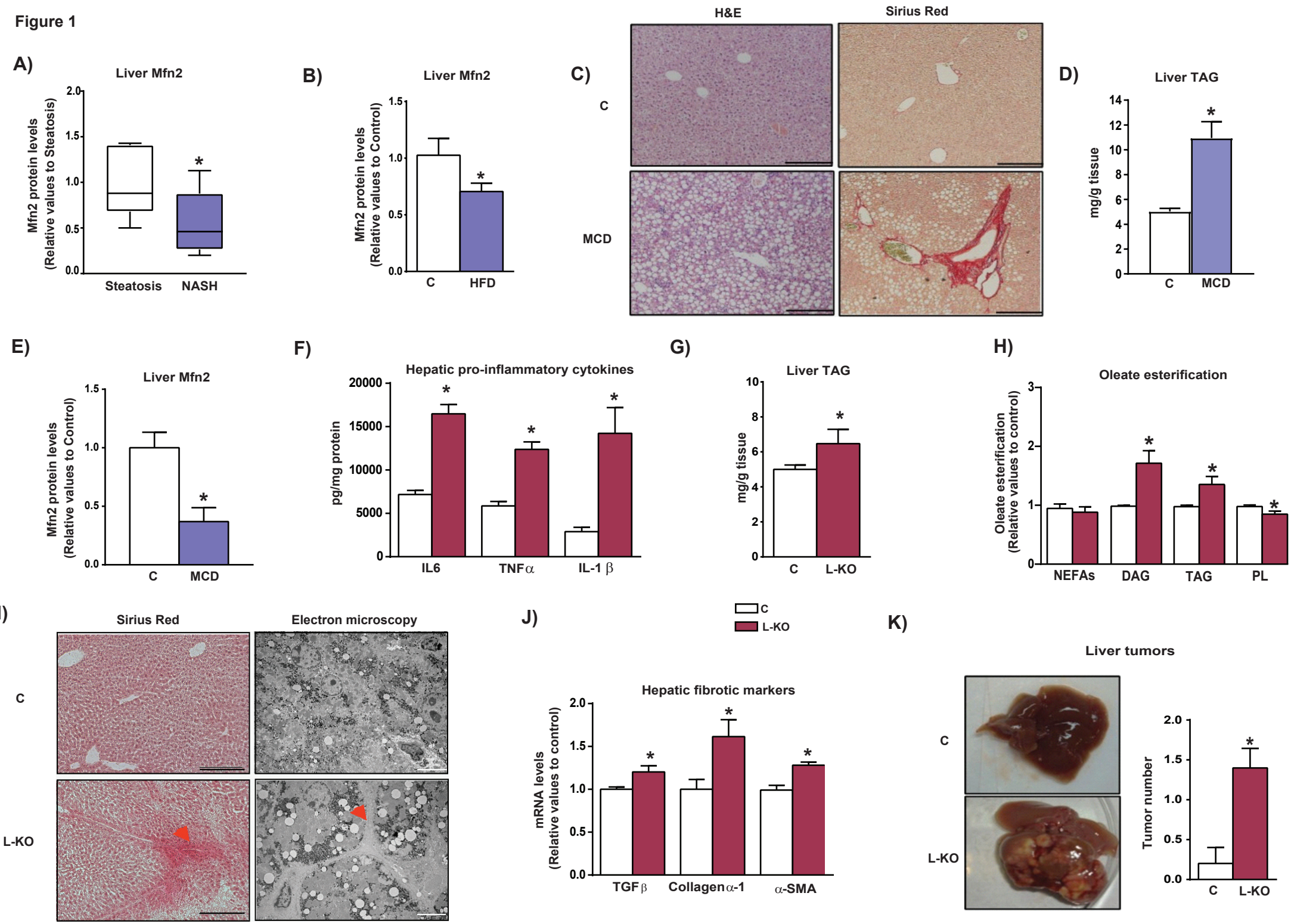
A)
Liver Mfn2
Mfn2 protein levels (Relative values to Steatosis)
2.0
1.5
1.0
0.5
0.0
*
Steatosis
NASH
B)
Liver Mfn2
Mfn2 protein levels (Relative values to Control)
1.5
1.0
0.5
0.0
*
C
HFD
C)
H&E
Sirius Red
C
MCD
D)
Liver TAG
mg/g tissue
14
12
10
8
6
4
2
0
*
C
MCD
E)
Liver Mfn2
Mfn2 protein levels (Relative values to Control)
1.5
1.0
0.5
0.0
*
C
MCD
F)
Hepatic pro-inflammatory cytokines
pg/mg protein
20000
15000
10000
5000
0
*
*
*
IL6
TNFα
IL-1 β
G)
Liver TAG
mg/g tissue
10
8
6
4
2
0
*
C
L-KO
H)
Oleate esterification
Oleate esterification (Relative values to control)
3
2
1
0
*
*
*
NEFAs
DAG
TAG
PL
I)
Sirius Red
Electron microscopy
C
L-KO
J)
C
L-KO
Hepatic fibrotic markers
mRNA levels (Relative values to control)
2.0
1.5
1.0
0.5
0.0
*
*
*
TGF β
Collagen α-1
α-SMA
K)
Liver tumors
C
L-KO
Tumor number
2.0
1.5
1.0
0.5
0.0
*
C
L-KO

Figure 2

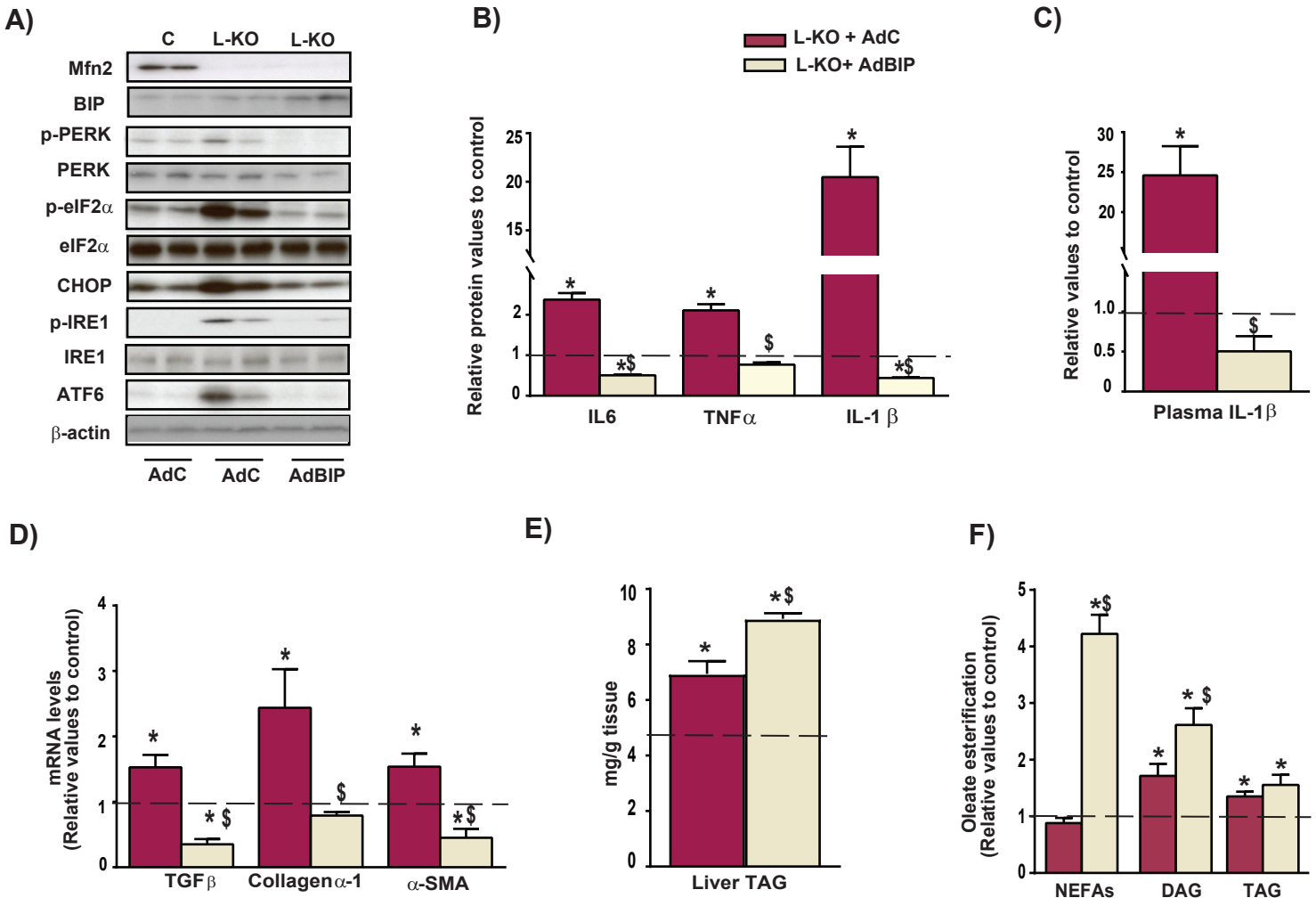
A)
C
L-KO
L-KO
Mfn2
BIP
p-PERK
PERK
p-eIF2α
eIF2α
CHOP
p-IRE1
IRE1
ATF6
β-actin
AdC
AdC
AdBIP
B)
L-KO + AdC
L-KO+ AdBIP
Relative protein values to control
IL6
TNFα
IL-1 β
C)
Relative values to control
Plasma IL-1β
D)
mRNA levels
(Relative values to control)
TGFβ
Collagen α-1
α-SMA
E)
mg/g tissue
Liver TAG
F)
Oleate esterification
(Relative values to control)
NEFAs
DAG
TAG

Figure 3

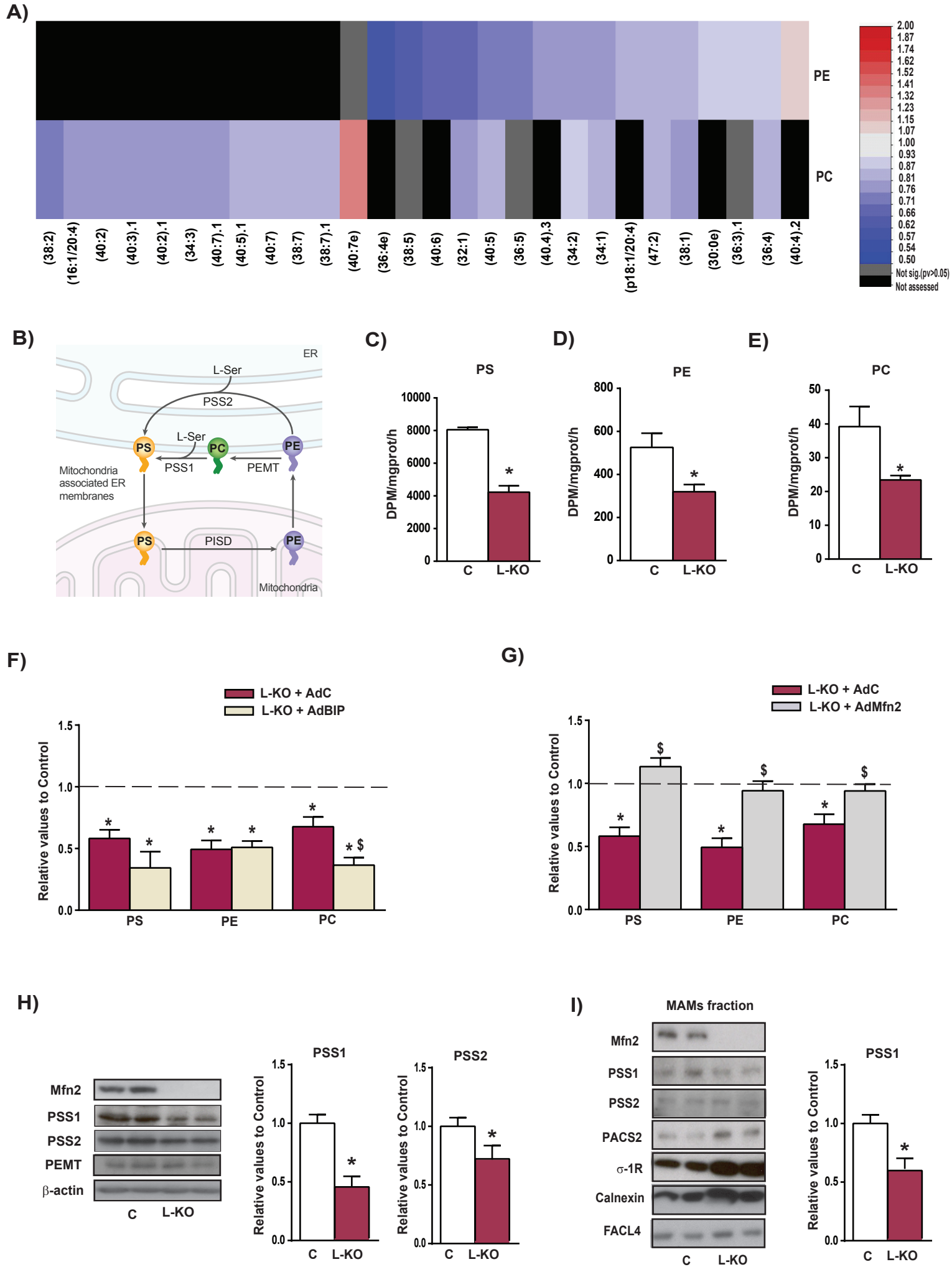
A)
PE
PC
2.00
1.87
1.74
1.62
1.52
1.41
1.32
1.23
1.15
1.07
1.00
0.93
0.87
0.81
0.76
0.71
0.66
0.62
0.57
0.54
0.50
Not sig.(pv>0.05)
Not assessed
(38:2)
(16:1/20:4)
(40:2)
(40:3).1
(40:2).1
(34:3)
(40:7).1
(40:5).1
(40:7)
(38:7)
(38:7).1
(40:7e)
(36:4e)
(38:5)
(40:6)
(32:1)
(40:5)
(36:5)
(40.4).3
(34:2)
(34:1)
(p18:1/20:4)
(47:2)
(38:1)
(30:0e)
(36:3).1
(36:4)
(40:4).2
B)
ER
L-Ser
PSS2
L-Ser
PS
PC
PE
PSS1
PEMT
Mitochondria associated ER membranes
PS
PISD
PE
Mitochondria
C)
PS
DPM/mgprot/h
10000
8000
6000
4000
2000
0
C
L-KO
D)
PE
DPM/mgprot/h
800
600
400
200
0
C
L-KO
E)
PC
DPM/mgprot/h
50
40
30
20
10
0
C
L-KO
F)
L-KO + AdC
L-KO + AdBIP
Relative values to Control
1.5
1.0
0.5
0.0
PS
PE
PC
G)
L-KO + AdC
L-KO + AdMfn2
Relative values to Control
1.5
1.0
0.5
0.0
PS
PE
PC
H)
Mfn2
PSS1
PSS2
PEMT
β-actin
C
L-KO
PSS1
Relative values to Control
1.5
1.0
0.5
0.0
C
L-KO
PSS2
Relative values to Control
1.5
1.0
0.5
0.0
C
L-KO
I)
MAMs fraction
Mfn2
PSS1
PSS2
PACS2
σ-1R
Calnexin
FACL4
C
L-KO
PSS1
Relative values to Control
1.5
1.0
0.5
0.0
C
L-KO

Figure 4

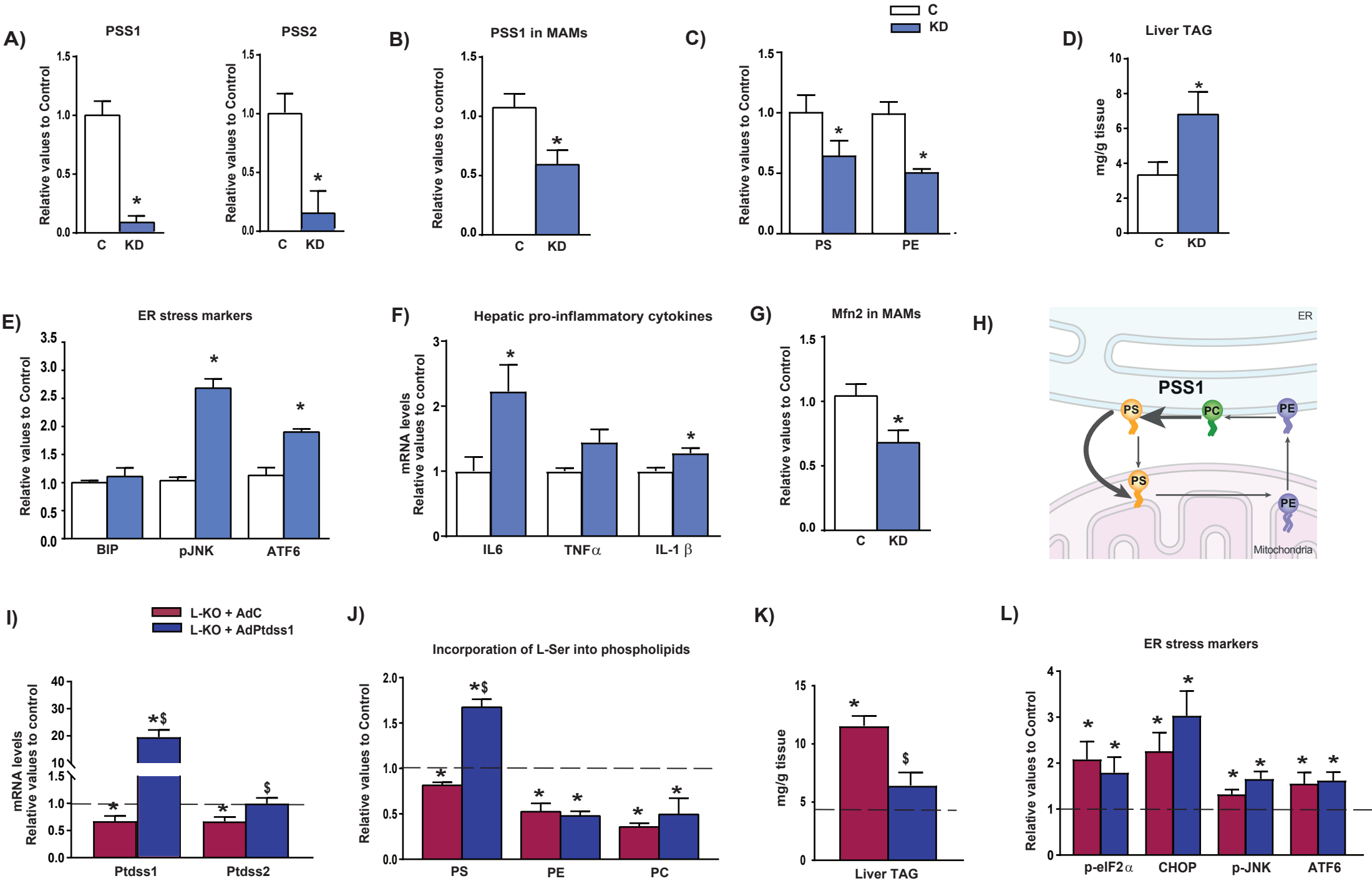
A)
PSS1
PSS2
Relative values to Control
C
KD
B)
PSS1 in MAMs
Relative values to control
C)
C
KD
PS
PE
D)
Liver TAG
mg/g tissue
E)
ER stress markers
BIP
pJNK
ATF6
F)
Hepatic pro-inflammatory cytokines
mRNA levels
Relative values to control
IL6
TNFα
IL-1 β
G)
Mfn2 in MAMs
H)
ER
PSS1
PS
PC
PE
Mitochondria
I)
L-KO + AdC
L-KO + AdPtdss1
Ptdss1
Ptdss2
J)
Incorporation of L-Ser into phospholipids
PS
PE
PC
K)
Liver TAG
L)
ER stress markers
p-eIF2α
CHOP
p-JNK
ATF6

Figure 5

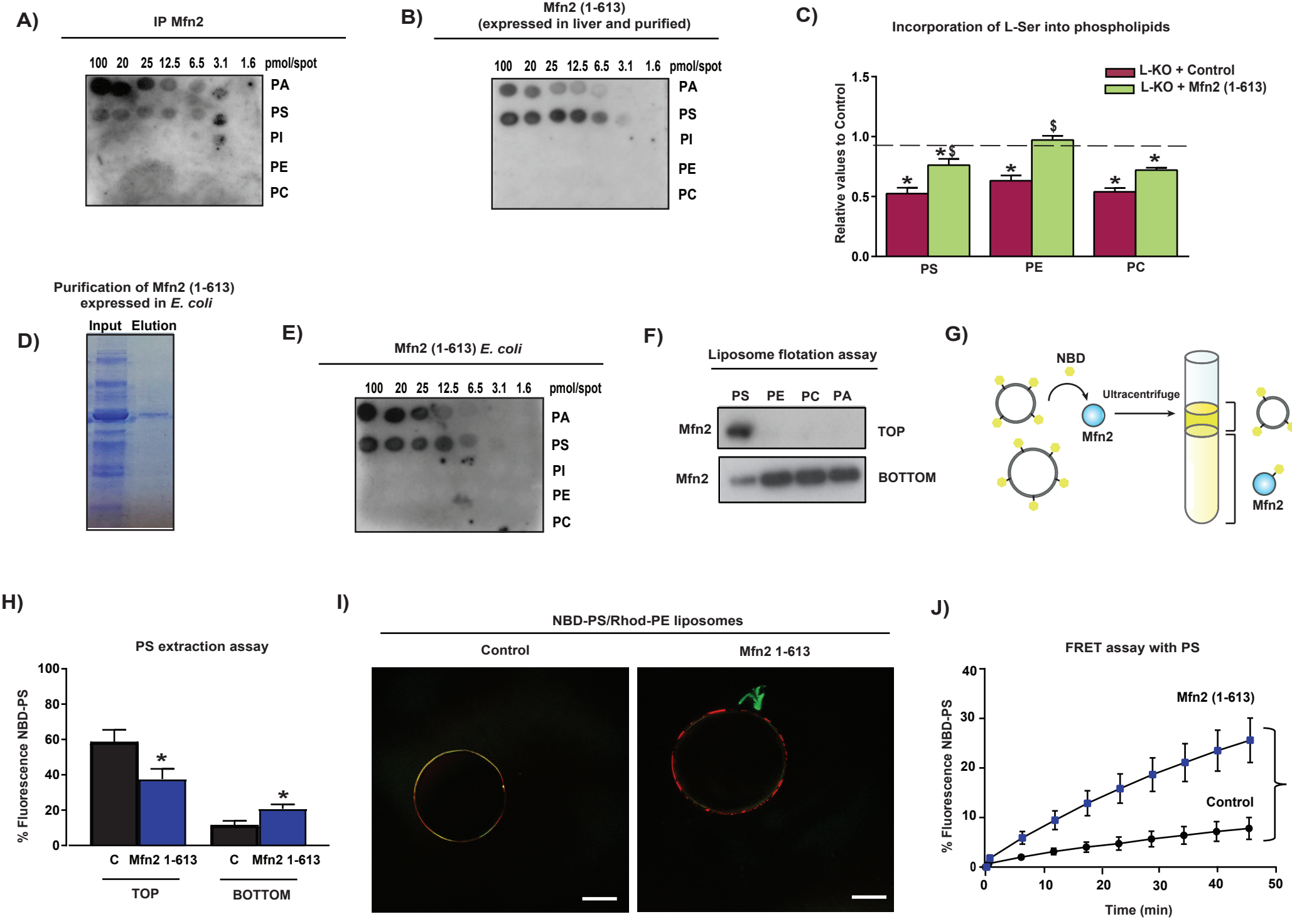
A)
IP Mfn2
100 20 25 12.5 6.5 3.1 1.6 pmol/spot
PA
PS
PI
PE
PC
B)
Mfn2 (1-613)
(expressed in liver and purified)
100 20 25 12.5 6.5 3.1 1.6 pmol/spot
PA
PS
PI
PE
PC
C)
Incorporation of L-Ser into phospholipids
L-KO + Control
L-KO + Mfn2 (1-613)
Relative values to Control
1.5
1.0
0.5
0.0
PS
PE
PC
Purification of Mfn2 (1-613)
expressed in E. coli
D)
Input Elution
E)
Mfn2 (1-613) E. coli
100 20 25 12.5 6.5 3.1 1.6 pmol/spot
PA
PS
PI
PE
PC
F)
Liposome flotation assay
PS PE PC PA
Mfn2
TOP
Mfn2
BOTTOM
G)
NBD
Ultracentrifuge
Mfn2
Mfn2
H)
PS extraction assay
% Fluorescence NBD-PS
100
80
60
40
20
0
C Mfn2 1-613 C Mfn2 1-613
TOP
BOTTOM
I)
NBD-PS/Rhod-PE liposomes
Control
Mfn2 1-613
J)
FRET assay with PS
% Fluorescence NBD-PS
40
30
20
10
0
Mfn2 (1-613)
Control
0 10 20 30 40 50
Time (min)

Figure 6

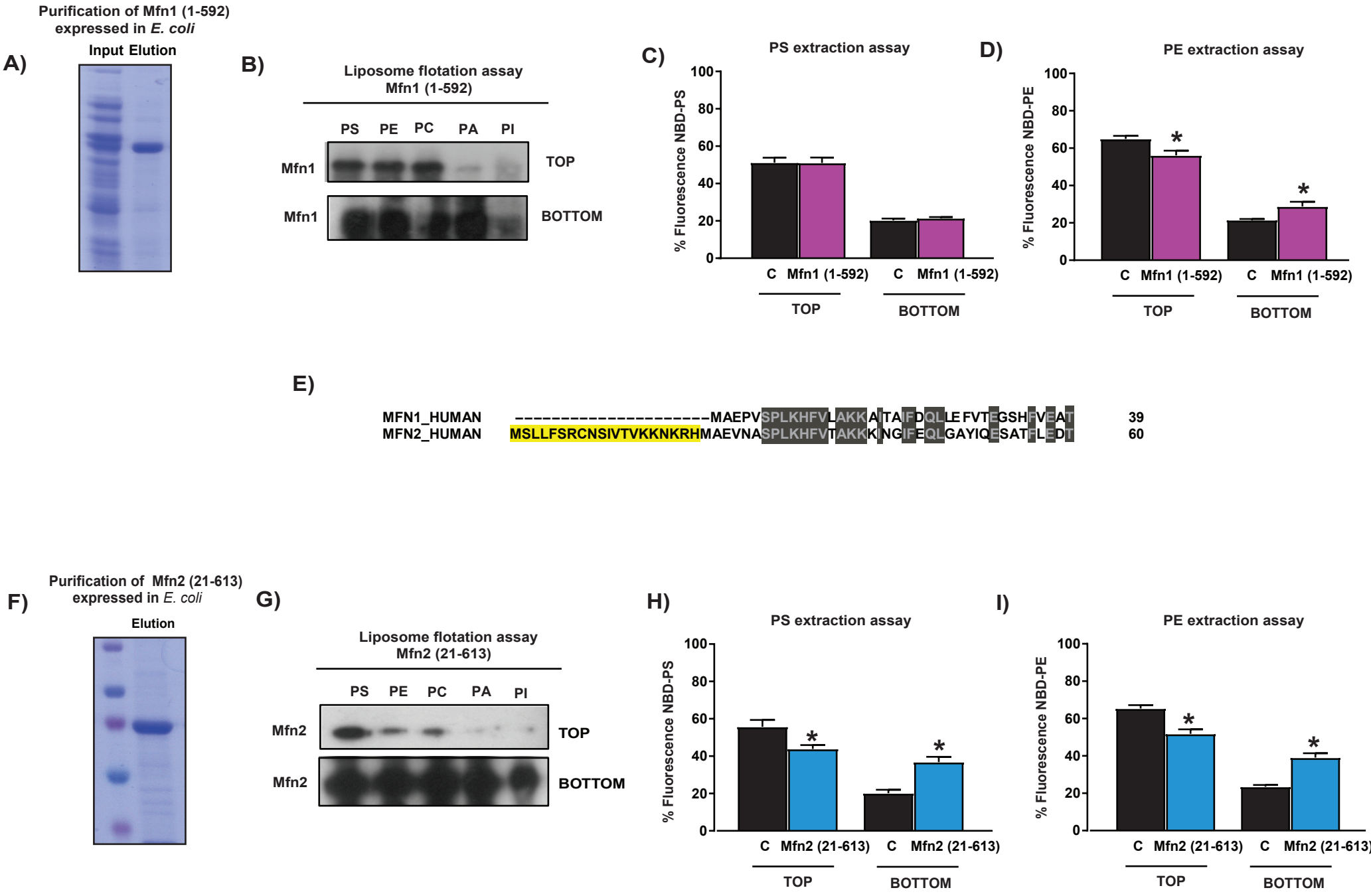
Purification of Mfn1 (1-592) expressed in E. coli
Input Elution
A)
B)
Liposome flotation assay
Mfn1 (1-592)
PS PE PC PA PI
Mfn1
TOP
Mfn1
BOTTOM
C)
PS extraction assay
% Fluorescence NBD-PS
100
80
60
40
20
0
C Mfn1 (1-592) C Mfn1 (1-592)
TOP
BOTTOM
D)
PE extraction assay
% Fluorescence NBD-PE
100
80
60
40
20
0
C Mfn1 (1-592) C Mfn1 (1-592)
TOP
BOTTOM
E)
MFN1_HUMAN ----------MAEPV
MFN2_HUMAN MSLLFSRCNSIVTVKKNKRHMAEVNA
39
60
F)
Purification of Mfn2 (21-613) expressed in E. coli
Elution
G)
Liposome flotation assay
Mfn2 (21-613)
PS PE PC PA PI
Mfn2
TOP
Mfn2
BOTTOM
H)
PS extraction assay
% Fluorescence NBD-PS
100
80
60
40
20
0
C Mfn2 (21-613) C Mfn2 (21-613)
TOP
BOTTOM
I)
PE extraction assay
% Fluorescence NBD-PE
100
80
60
40
20
0
C Mfn2 (21-613) C Mfn2 (21-613)
TOP
BOTTOM

Figure 7

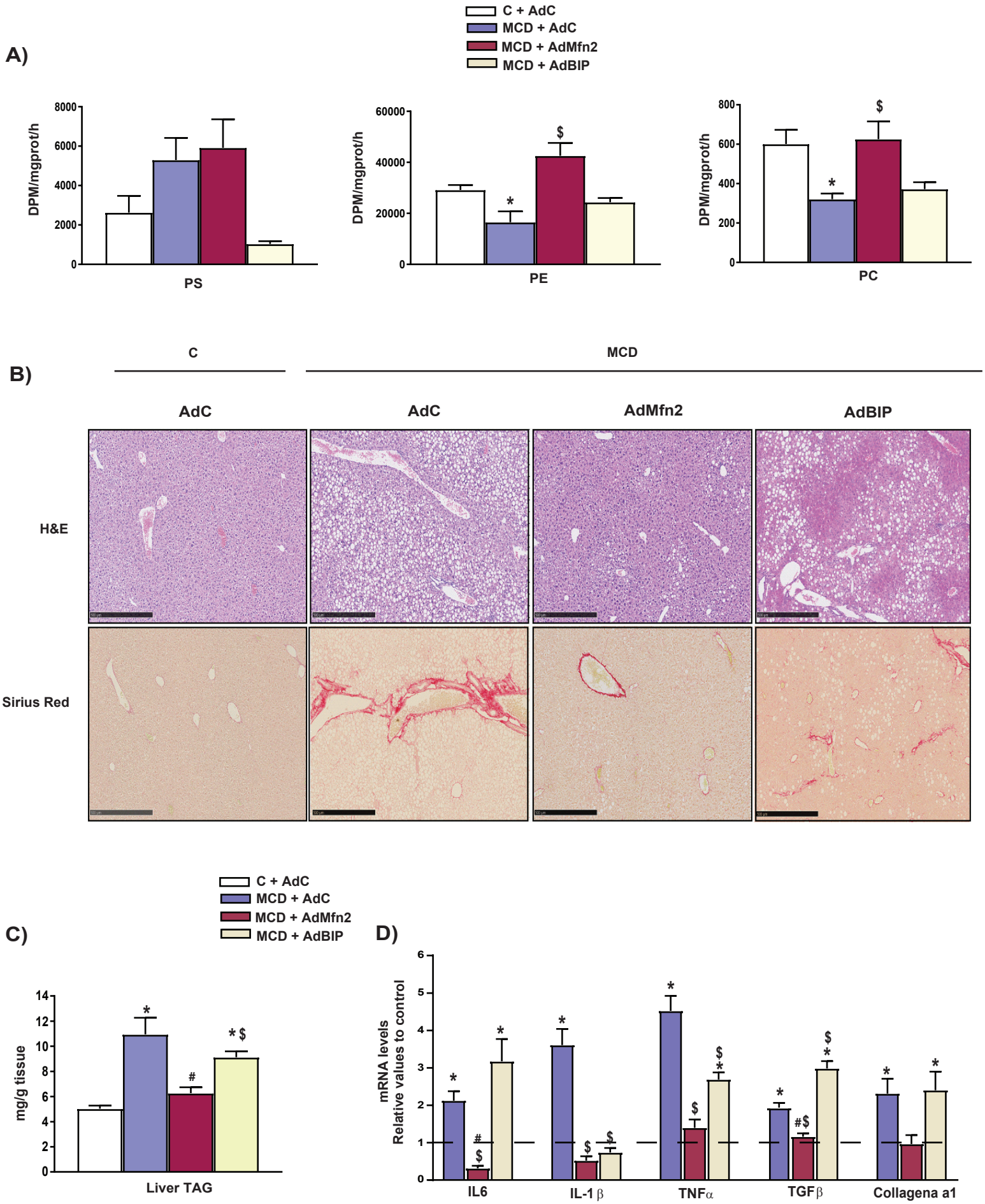
A)
C + AdC
MCD + AdC
MCD + AdMfn2
MCD + AdBIP
DPM/mgprot/h
PS
PE
PC
B)
C
MCD
AdC
AdC
AdMfn2
AdBIP
H&E
Sirius Red
C)
mg/g tissue
Liver TAG
D)
mRNA levels
Relative values to control
IL6
IL-1 β
TNFα
TGFβ
Collagena a1

SUPPLEMENTARY DATA

Figura S1

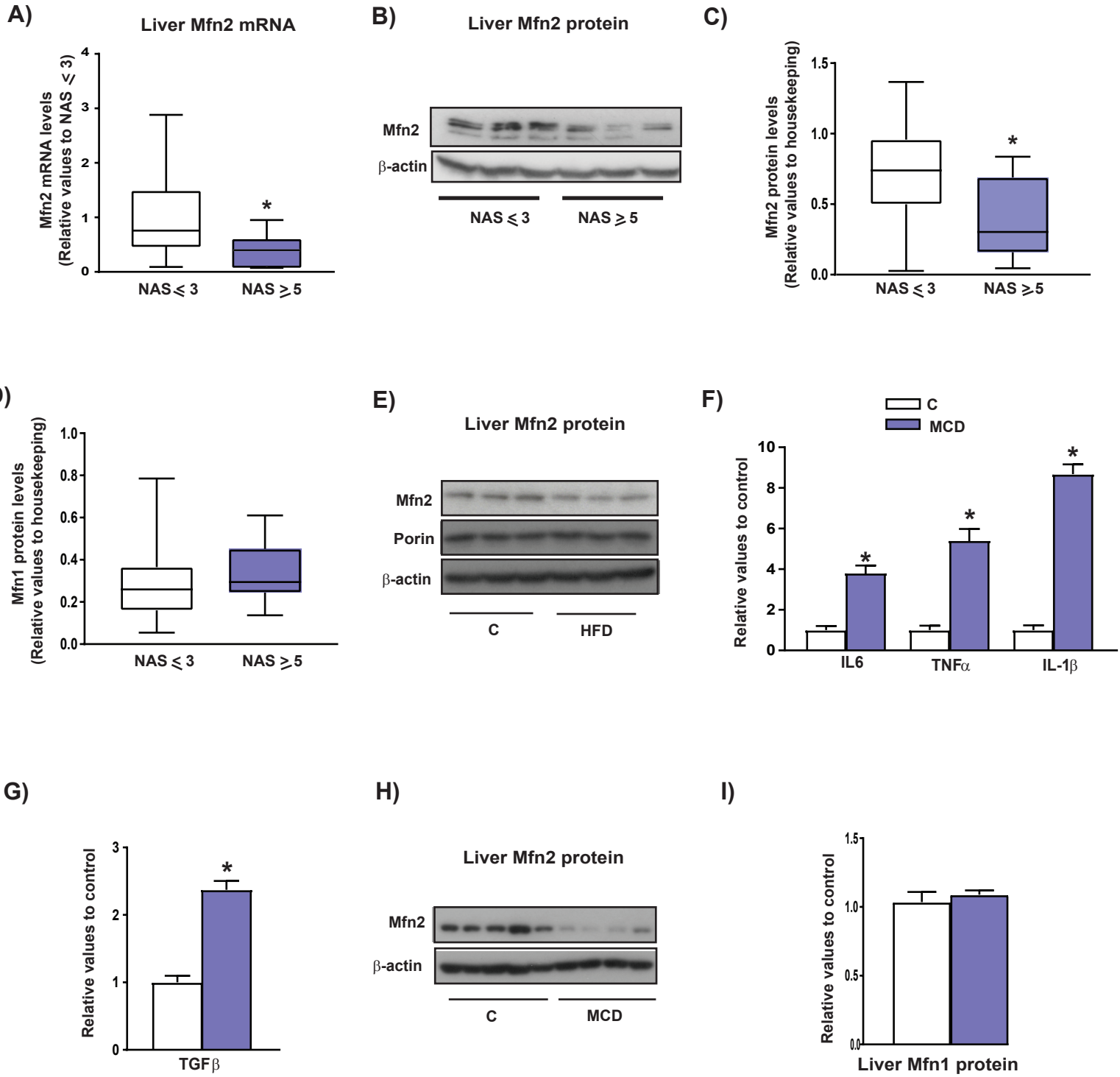
A)
Liver Mfn2 mRNA
Mfn2 mRNA levels
(Relative values to NAS ⩽ 3)
NAS ⩽ 3
NAS ⩾ 5
B)
Liver Mfn2 protein
Mfn2
β-actin
NAS ⩽ 3
NAS ⩾ 5
C)
Mfn2 protein levels
(Relative values to housekeeping)
NAS ⩽ 3
NAS ⩾ 5
D)
Mfn1 protein levels
(Relative values to housekeeping)
NAS ⩽ 3
NAS ⩾ 5
E)
Liver Mfn2 protein
Mfn2
Porin
β-actin
C
HFD
F)
C
MCD
Relative values to control
IL6
TNFα
IL-1β
G)
Relative values to control
TGFβ
H)
Liver Mfn2 protein
Mfn2
β-actin
C
MCD
I)
Relative values to control
Liver Mfn1 protein

FIGURE S1. Mfn2 is downregulated in NASH. A) mRNA levels of *Mfn2* in liver biopsies from NAS ≤ 3 (n=8) and NAS ≥ 5 subjects (n=8). B) Representative western blot of Mfn2 protein in liver biopsies from NAS ≤ 3 and NAS ≥ 5 subjects. C) Quantification of Mfn2 protein in liver biopsies from NAS ≤ 3 and NAS ≥ 5 subjects (n=20 per group). D) Quantification of Mfn1 protein in liver biopsies from NAS ≤ 3 and NAS ≥ 5 subjects (n=20 per group). E) Representative western blot of Mfn2 protein from mice on chow diet (C) or high-fat diet (HFD, model of steatosis). F) mRNA levels of pro-inflammatory markers from liver from mice on (C) or methionine/choline-deficient diet combined with high-fat diet and supplemented with 0.1% L-methionine in drinking water (MCD) (n=4 mice per group). G) mRNA levels of TGFβ from C and MCD mice (n=4 mice per group). H) Representative western blot of Mfn2 protein from C and MCD mice (n=5 mice per group). I) Quantification of Mfn1 protein levels from C and MCD mice (n=4 mice per group). Data in A–D are expressed as mean ± SD. Data in E–I are expressed as mean ± SE. *$p<0.05$ vs. C.

Figure S2

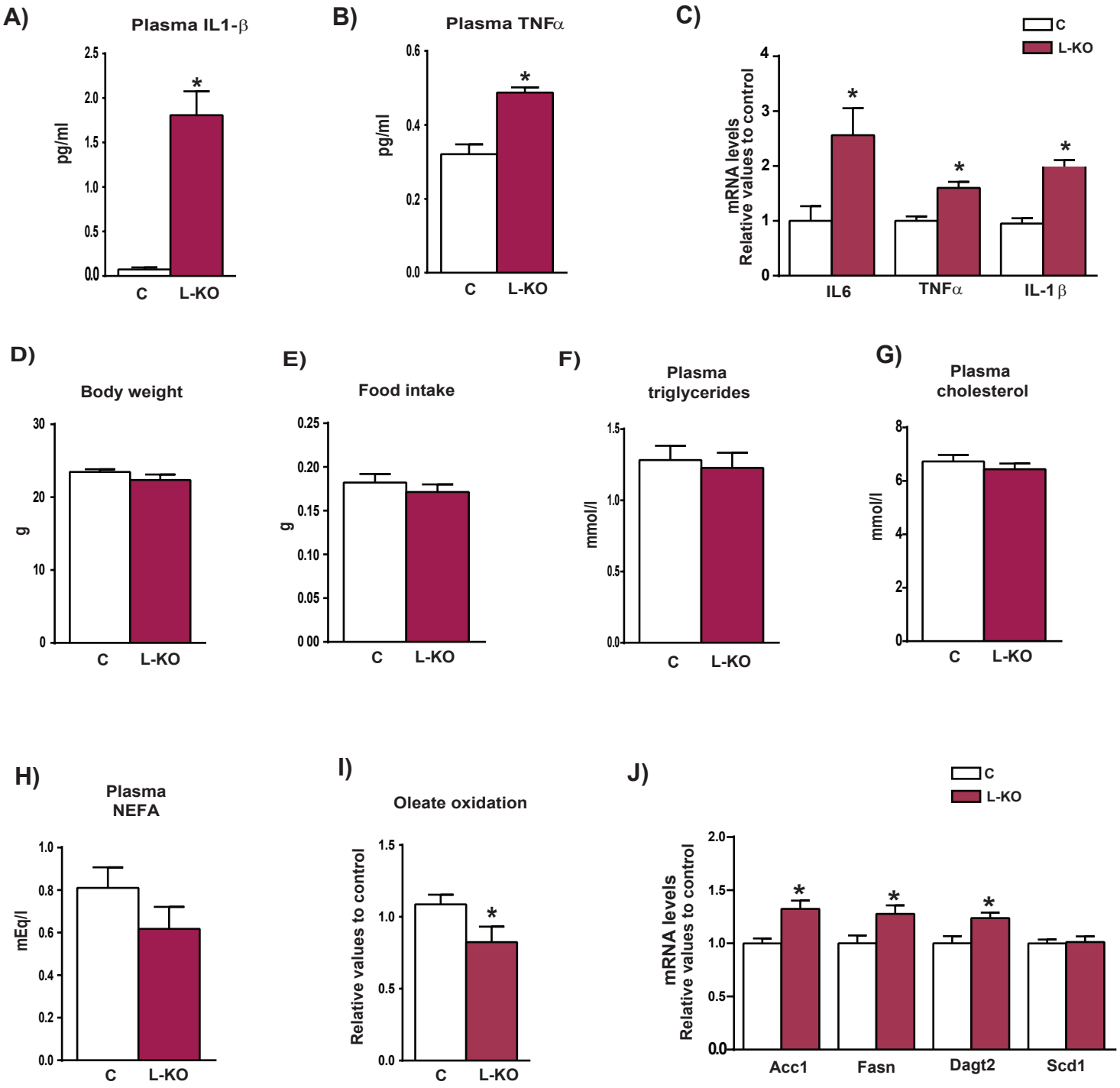
A)
Plasma IL1-β
pg/ml
2.5
2.0
1.5
1.0
0.5
0.0
*
C
L-KO
B)
Plasma TNFα
pg/ml
0.6
0.4
0.2
0.0
*
C
L-KO
C)
C
L-KO
mRNA levels
Relative values to control
4
3
2
1
0
*
*
*
IL6
TNFα
IL-1β
D)
Body weight
g
30
20
10
0
C
L-KO
E)
Food intake
g
0.25
0.20
0.15
0.10
0.05
0 00
C
L-KO
F)
Plasma
triglycerides
mmol/l
1.5
1.0
0.5
0.0
C
L-KO
G)
Plasma
cholesterol
mmol/l
8
6
4
2
0
C
L-KO
H)
Plasma
NEFA
mEq/l
1.0
0.8
0.6
0.4
0.2
0.0
C
L-KO
I)
Oleate oxidation
Relative values to control
1.5
1.0
0.5
0.0
*
C
L-KO
J)
C
L-KO
mRNA levels
Relative values to control
2.0
1.5
1.0
0.5
0.0
*
*
*
Acc1
Fasn
Dagt2
Scd1

FIGURE S2. Phenotype of liver-specific Mfn2 knockout mice. Eight week-old control (C) and L-KO mice were used unless stated otherwise. Control mice are represented as open bars and L-KO mice as red bars. A, B) Plasma levels of pro-inflammatory markers (n=8–12 mice per group). C) Hepatic expression of pro-inflammatory genes (n=8–12 mice per group). D) Body weight of C and L-KO mice (n=8–12 mice per group). E) Food intake of C and L-KO mice (n=8–12 mice per group). F–H) Plasma concentrations of lipid metabolites (n=8–12 mice per group). I) Oleate oxidation in isolated hepatocytes from C and L-KO mice (n=6 mice per group; each experiment performed in triplicate). J) mRNA levels of genes involved in lipid metabolism (n=8–12 mice per group). Data are expressed as mean ± SE. *$p<0.05$ vs. C.

Figure S3

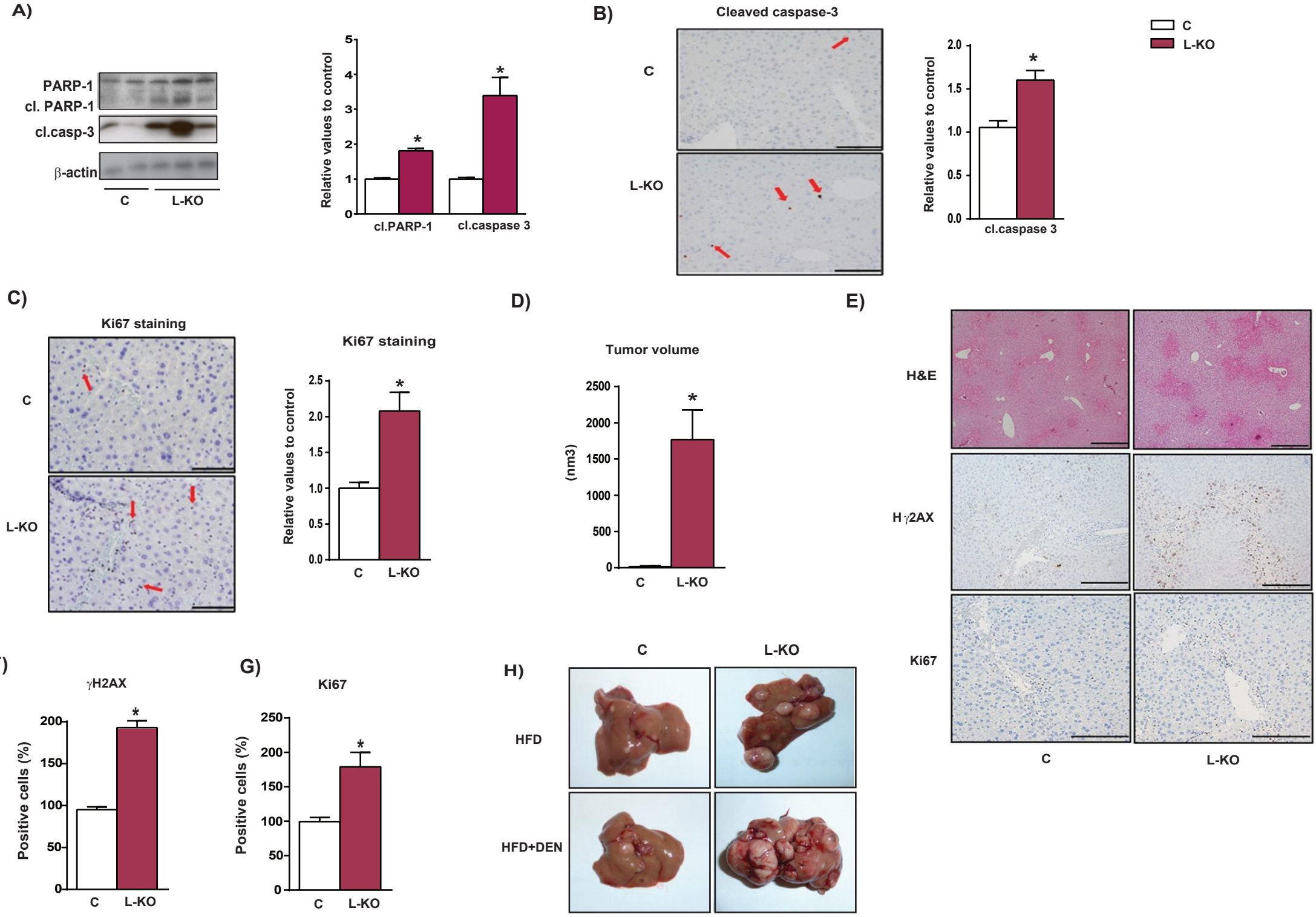
A)
PARP-1
cl. PARP-1
cl.casp-3
β-actin
C
L-KO
Relative values to control
cl.PARP-1
cl.caspase 3
B)
Cleaved caspase-3
C
L-KO
Relative values to control
cl.caspase 3
C)
Ki67 staining
C
L-KO
Ki67 staining
Relative values to control
D)
Tumor volume
(nm3)
E)
H&E
H γ2AX
Ki67
F)
γH2AX
Positive cells (%)
G)
Ki67
Positive cells (%)
H)
HFD
HFD+DEN

FIGURE S3. Mfn2 ablation causes apoptosis, increased cell growth, and liver cancer. A) Representative western and protein quantification of apoptosis markers in liver from control (C) and L-KO mice (n=4 mice per group). B) Representative images (scale bar, 100 μm) and quantification of cleaved caspase 3 in liver sections from C and L-KO mice (n=6 mice per group). C) Representative images and quantification (scale bar, 100 μm) of Ki67 in liver sections from C and L-KO mice (n=6 mice per group). D) Mean tumor volume measured in livers from 24-month-old C and L-KO mice (n=5 mice per group). E) Representative images (scale bar, 200 μm) of H&E, γH2AX (DNA damage marker) and Ki67 (proliferation marker) staining in liver sections from C and L-KO mice acutely treated with diethylnitrosamine (DEN) (50 mg/kg for 48 h, n=5 mice per group). F,G) Quantification of γH2AX and Ki67 in liver sections from 12 week-old C and L-KO mice acutely treated with a high dose of diethylnitrosamine (DEN) (n=5 mice per group). H) Representative liver macroscopic images from C and L-KO mice treated for 7 months with HFD or HFD+DEN (5 mg/kg). Data are expressed as mean ± SE. *$p<0.05$ vs. C.

Figure S4

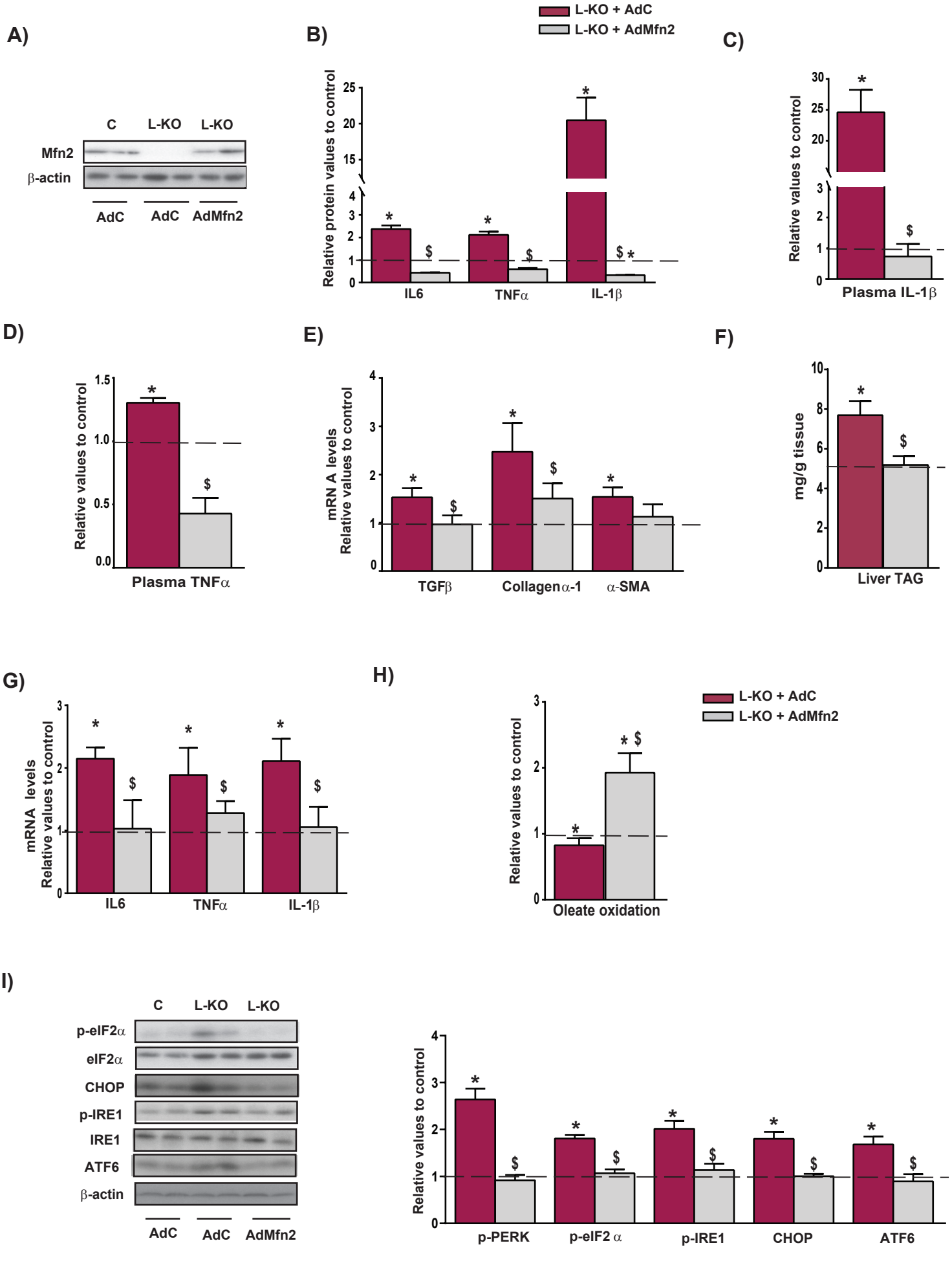
A)
C
L-KO
L-KO
Mfn2
β-actin
AdC
AdC
AdMfn2
B)
L-KO + AdC
L-KO + AdMfn2
Relative protein values to control
IL6
TNFα
IL-1β
C)
Relative values to control
Plasma IL-1β
D)
Relative values to control
Plasma TNFα
E)
mRNA A levels
Relative values to control
TGFβ
Collagen α-1
α-SMA
F)
mg/g tissue
Liver TAG
G)
mRNA levels
Relative values to control
IL6
TNFα
IL-1β
H)
L-KO + AdC
L-KO + AdMfn2
Relative values to control
Oleate oxidation
I)
C
L-KO
L-KO
p-eIF2α
eIF2α
CHOP
p-IRE1
IRE1
ATF6
β-actin
AdC
AdC
AdMfn2
Relative values to control
p-PERK
p-eIF2 α
p-IRE1
CHOP
ATF6

FIGURE S4. Mfn2 re-expression restores normal liver metabolism in L-KO mice. Control mice were examined 5 days after tail vein injection of control LacZ adenoviruses (C+AdC) and L-KO mice were studied 5 days after tail vein injection of control (LacZ) (L-KO+AdC, red bars) or Mfn2 adenoviruses (L-KO+Mfn2, grey bars) (n=4 mice per group). Data are expressed as values relative to C+AdC group (shown as a discontinuous line). A) Representative western blot of Mfn2 protein in liver B) Hepatic levels of hepatic pro-inflammatory factors measured by ELISA. C,D) Plasma levels of the pro-inflammatory factors IL-1β and TNFα. E) Hepatic expression of genes involved in collagen synthesis. F) Triglyceride content in liver. G) Hepatic expression of pro-inflammatory genes. H) Oleate oxidation in isolated hepatocytes (n=4 mice per group, each experiment performed in triplicate). I) Representative western blot and quantification of hepatic ER stress markers. Data are expressed as mean ± SE. Statistical analysis was performed by using one-way ANOVA followed by post-hoc t tests. *$p<0.05$ vs. C+AdC, $^{\$}p<0.05$ L-KO+AdC.

Figure S5

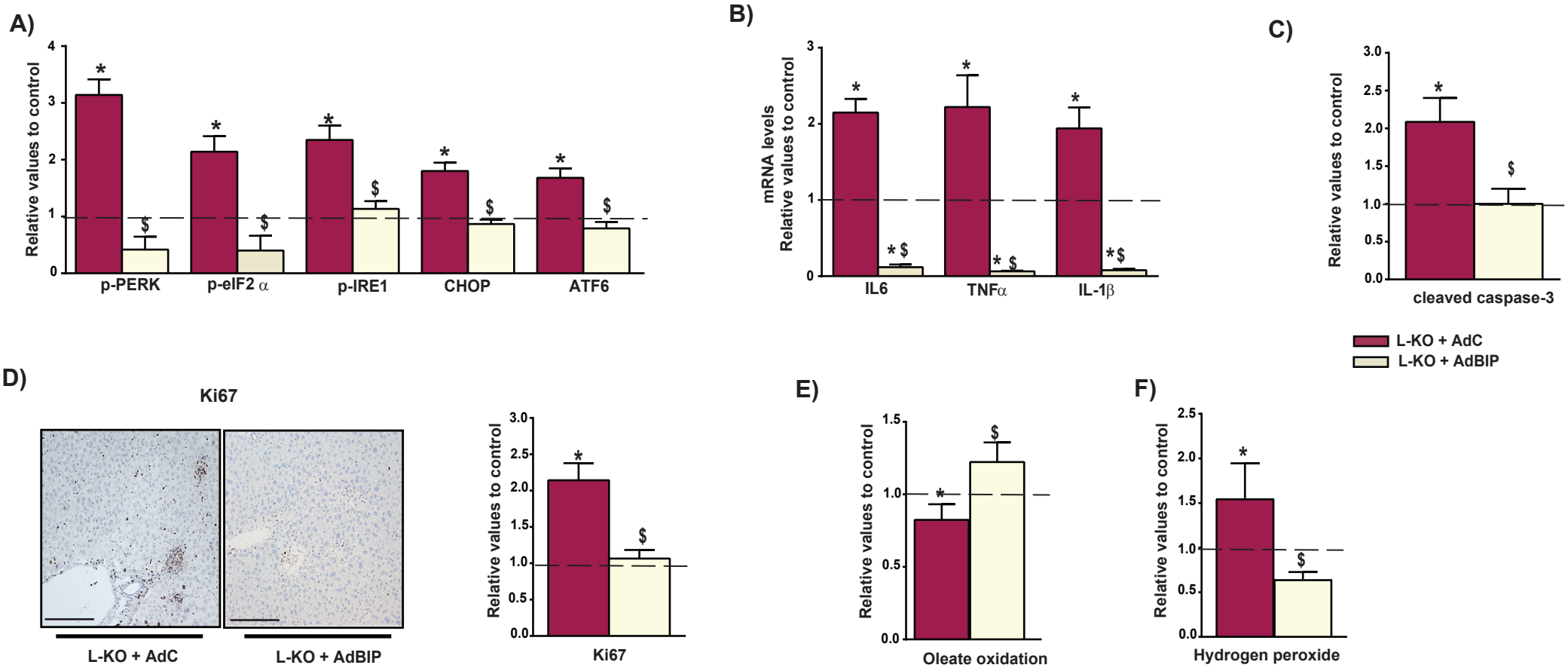
A)
Relative values to control
p-PERK
p-eIF2 α
p-IRE1
CHOP
ATF6
B)
mRNA levels
Relative values to control
IL6
TNFα
IL-1β
C)
Relative values to control
cleaved caspase-3
L-KO + AdC
L-KO + AdBIP
D)
Ki67
L-KO + AdC
L-KO + AdBIP
Relative values to control
Ki67
E)
Relative values to control
Oleate oxidation
F)
Relative values to control
Hydrogen peroxide

FIGURE S5. Effect of normalization of ER stress in L-KO mice. Control mice were studied 5 days after tail vein injection of control LacZ adenoviruses (C+AdC) and L-KO mice were studied 5 days after tail vein injection of control (LacZ) (L-KO+AdC, red bars) or BIP adenoviruses (L-KO+AdBIP, yellow bars). Data are expressed as values relative to C+AdC group (shown as a discontinuous line). A) Quantification of hepatic ER stress markers (n=4 mice per group). B) Hepatic mRNA expression of pro-inflammatory genes (n=4 mice per group). C) Quantification of cleaved caspase 3 in liver sections (n=4 mice per group). D) Representative images (scale bar, 100 μm) and quantification of the proliferation marker Ki67 in liver sections (n=4 mice per group). E) Oleate oxidation in isolated hepatocytes (n=4 mice per group, each experiment performed in triplicate). F) Hepatic hydrogen peroxide levels (n=4 mice per group). Data are expressed as mean ± SE. Statistical analysis was performed by using one-way ANOVA followed by post-hoc t tests. *$p<0.05$ vs. control+AdC, $^{\$}p<0.05$ vs L-KO+AdC.

Figure S6

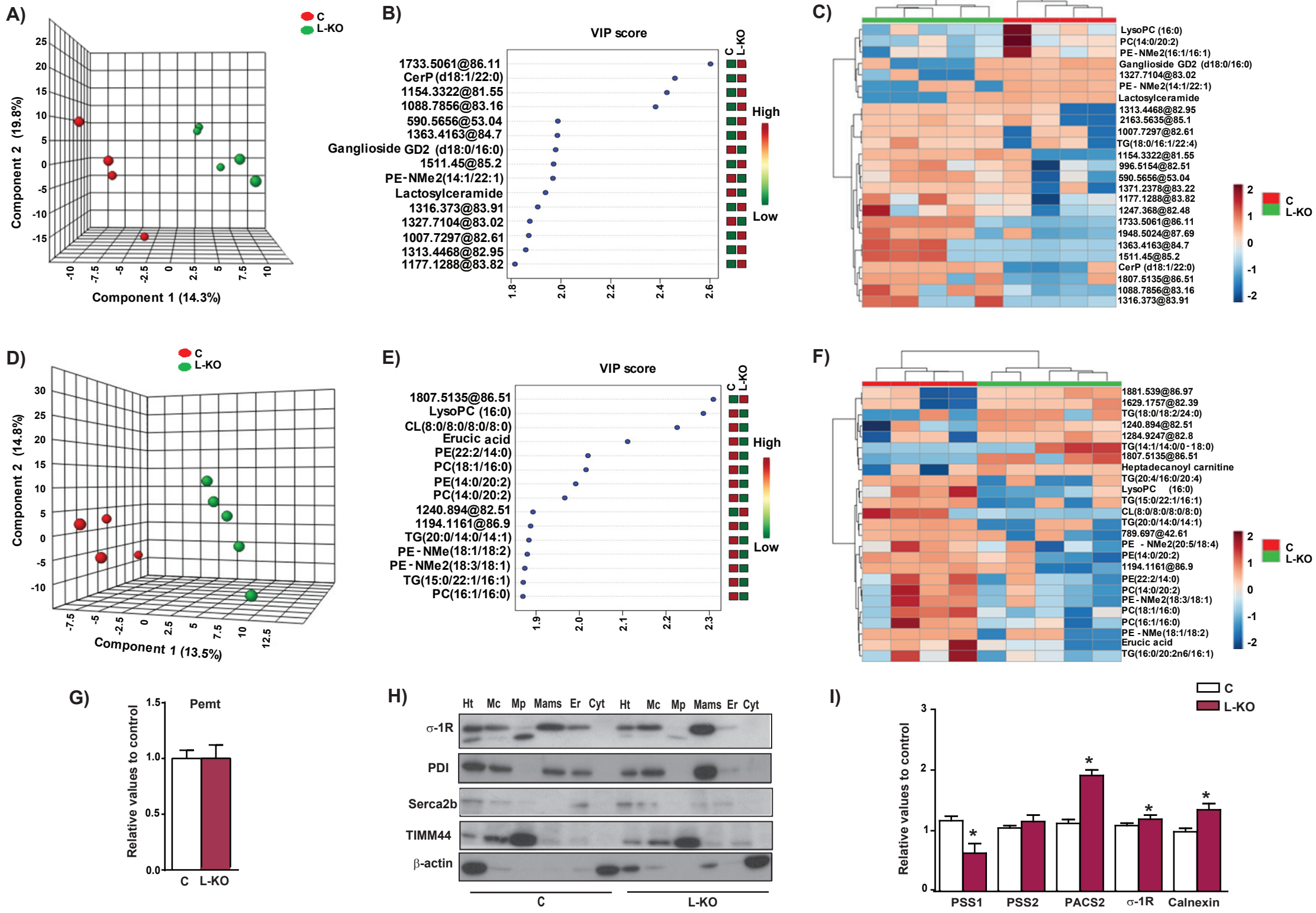
A)
C
L-KO
Component 2 (19.8%)
Component 1 (14.3%)
B)
VIP score
1733.5061@86.11
CerP (d18:1/22:0)
1154.3322@81.55
1088.7856@83.16
590.5656@53.04
1363.4163@84.7
Ganglioside GD2 (d18:0/16:0)
1511.45@85.2
PE-NMe2(14:1/22:1)
Lactosylceramide
1316.373@83.91
1327.7104@83.02
1007.7297@82.61
1313.4468@82.95
1177.1288@83.82
High
Low
C)
LysoPC (16:0)
PC(14:0/20:2)
PE-NMe2(16:1/16:1)
Ganglioside GD2 (d18:0/16:0)
1327.7104@83.02
PE-NMe2(14:1/22:1)
Lactosylceramide
1313.4468@82.95
2163.5635@85.1
1007.7297@82.61
TG(18:0/16:1/22:4)
1154.3322@81.55
996.5154@82.51
590.5656@53.04
1371.2378@83.22
1177.1288@83.82
1247.368@82.48
1733.5061@86.11
1948.5024@87.69
1363.4163@84.7
1511.45@85.2
CerP (d18:1/22:0)
1807.5135@86.51
1088.7856@83.16
1316.373@83.91
D)
C
L-KO
Component 2 (14.8%)
Component 1 (13.5%)
E)
VIP score
1807.5135@86.51
LysoPC (16:0)
CL(8:0/8:0/8:0/8:0)
Erucic acid
PE(22:2/14:0)
PC(18:1/16:0)
PE(14:0/20:2)
PC(14:0/20:2)
1240.894@82.51
1194.1161@86.9
TG(20:0/14:0/14:1)
PE-NMe(18:1/18:2)
PE-NMe2(18:3/18:1)
TG(15:0/22:1/16:1)
PC(16:1/16:0)
High
Low
F)
1881.539@86.97
1629.1757@82.39
TG(18:0/18:2/24:0)
1240.894@82.51
1284.9247@82.8
TG(14:1/14:0/0-18:0)
1807.5135@86.51
Heptadecanoyl carnitine
TG(20:4/16:0/20:4)
LysoPC (16:0)
TG(15:0/22:1/16:1)
CL(8:0/8:0/8:0/8:0)
TG(20:0/14:0/14:1)
789.697@42.61
PE-NMe2(20:5/18:4)
PE(14:0/20:2)
1194.1161@86.9
PE(22:2/14:0)
PC(14:0/20:2)
PE-NMe2(18:3/18:1)
PC(18:1/16:0)
PC(16:1/16:0)
PE-NMe(18:1/18:2)
Erucic acid
TG(16:0/20:2n6/16:1)
G)
Pemt
Relative values to control
C
L-KO
H)
Ht
Mc
Mp
Mams
Er
Cyt
σ-1R
PDI
Serca2b
TIMM44
β-actin
C
L-KO
I)
C
L-KO
Relative values to control
PSS1
PSS2
PACS2
σ-1R
Calnexin

FIGURE S6. Mfn2 ablation alters phospholipid metabolism and MAMs protein composition. Multivariate analyses revealed a specific lipidomic signature for KO mice compared with controls for both mitochondria (MIT) (A, B, C) and MAM (D, E, F). A, D) Partial Least Squares Discriminant Analyses (PLS-DA) showed a good clusterization of both groups according to their lipidomic profile. B, E). Variable Importance in Projection (VIP) scores represent those metabolites that contribute most to the PLS-DA model. C, F). Hierarchical clustering analyses using 25 metabolites with lowest p-values (Student's t-test) indicate a perfect clusterization between groups. Unknown identities are represented as exact mass@retention time. G) Hepatic PEMT protein expression in 8-week-old control and L-KO mice (n=4). H) Quality control of subcellular fractionation of livers obtained from 8-week-old control and L-KO mice. I) Abundance of protein markers in MAMs fractions obtained from control and L-KO mice (n=4). Data are expressed as mean ± SE. *$p<0.05$ vs. C+AdC, $^{\$}p<0.05$ vs. L-KO+AdC.

Figure S7

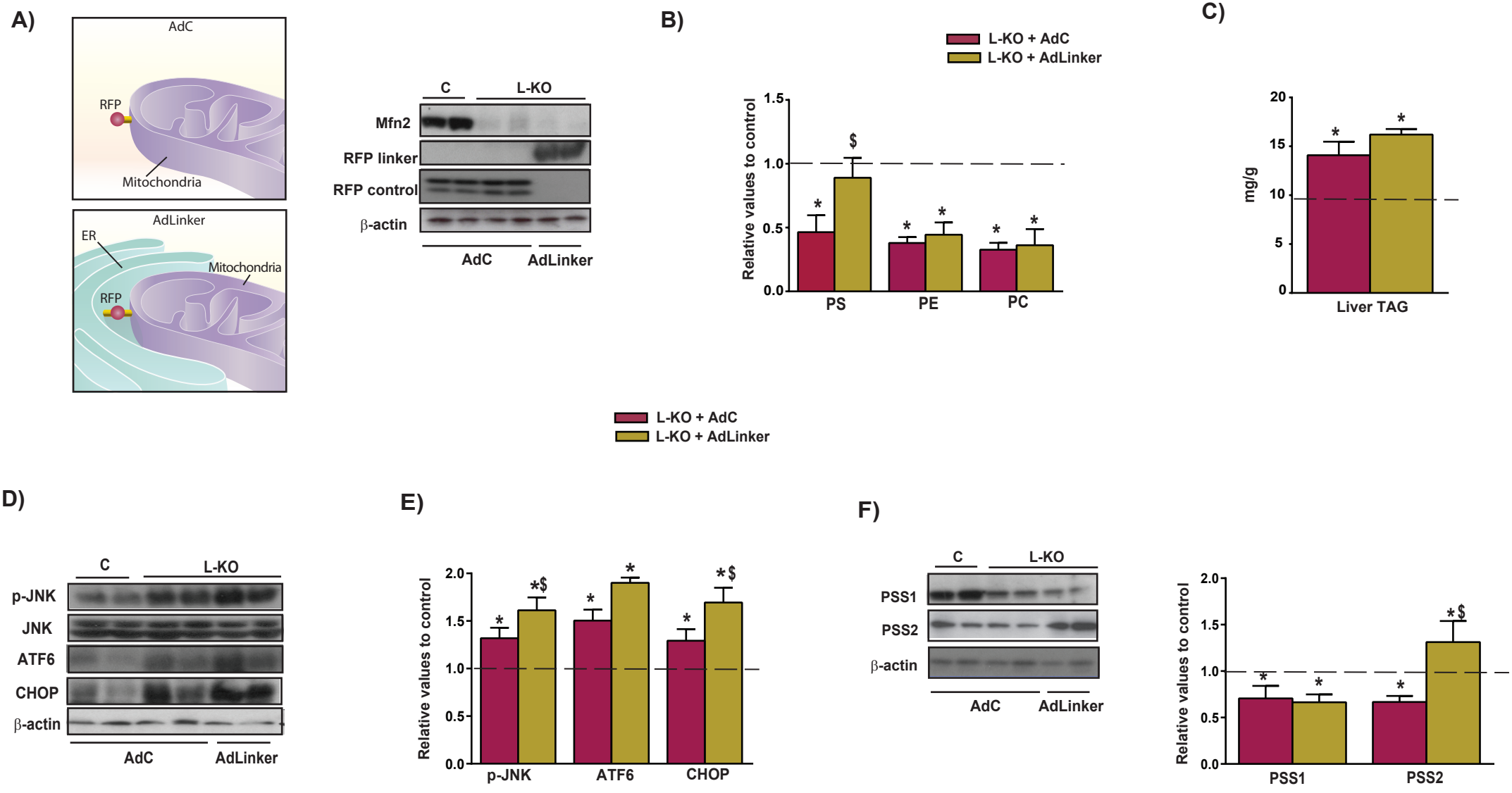
A)
AdC
RFP
Mitochondria
AdLinker
ER
Mitochondria
RFP
C
L-KO
Mfn2
RFP linker
RFP control
β-actin
AdC
AdLinker
B)
L-KO + AdC
L-KO + AdLinker
Relative values to control
1.5
1.0
0.5
0.0
$
*
PS
PE
PC
C)
mg/g
20
15
10
5
0
Liver TAG
L-KO + AdC
L-KO + AdLinker
D)
C
L-KO
p-JNK
JNK
ATF6
CHOP
β-actin
AdC
AdLinker
E)
Relative values to control
2.0
1.5
1.0
0.5
0.0
*$
p-JNK
ATF6
CHOP
F)
C
L-KO
PSS1
PSS2
β-actin
AdC
AdLinker
Relative values to control
PSS1
PSS2

FIGURE S7. Effect of ER-mitochondrial tethering in L-KO mice. Control (C) and L-KO livers were studied 5 days after tail vein injection of AdC or Adlinker (n=4 mice per group). A) Hepatic expression of RFP protein in C and L-KO mice after injection with control adenoviruses (C+AdC, L-KO+AdC) or with adenoviruses encoding a synthetic linker (C+AdLinker, L-KO+AdLinker). B) ^{3}H-L-serine incorporation into PS, PE and PC in hepatic mitochondria-associated ER-enriched fractions from C+AdC, L+KO+AdC (red bars) and L-KO+AdLinker (yellow bars). Data are expressed as values relative to C+AdC group (shown as a discontinuous line). C) Hepatic triglyceride levels from C+AdC, L+KO+AdC (red bars) and L-KO+AdLinker (yellow bars). D, E) Hepatic ER stress markers and quantification from C+AdC, L+KO+AdC (red bars) and L-KO+AdLinker (yellow bars). F) Representative western blot and quantification of hepatic PSS1 and PSS2 protein expression in C+AdC, L+KO+AdC (red bars) and L-KO+AdLinker (yellow bars) mice. Data are expressed as mean ± SE. Statistical analysis was performed by using one-way ANOVA followed by post-hoc t tests. *$p<0.05$ vs. C+AdC, $^{\$}p<0.05$ vs. L-KO+AdC.

Figure S8

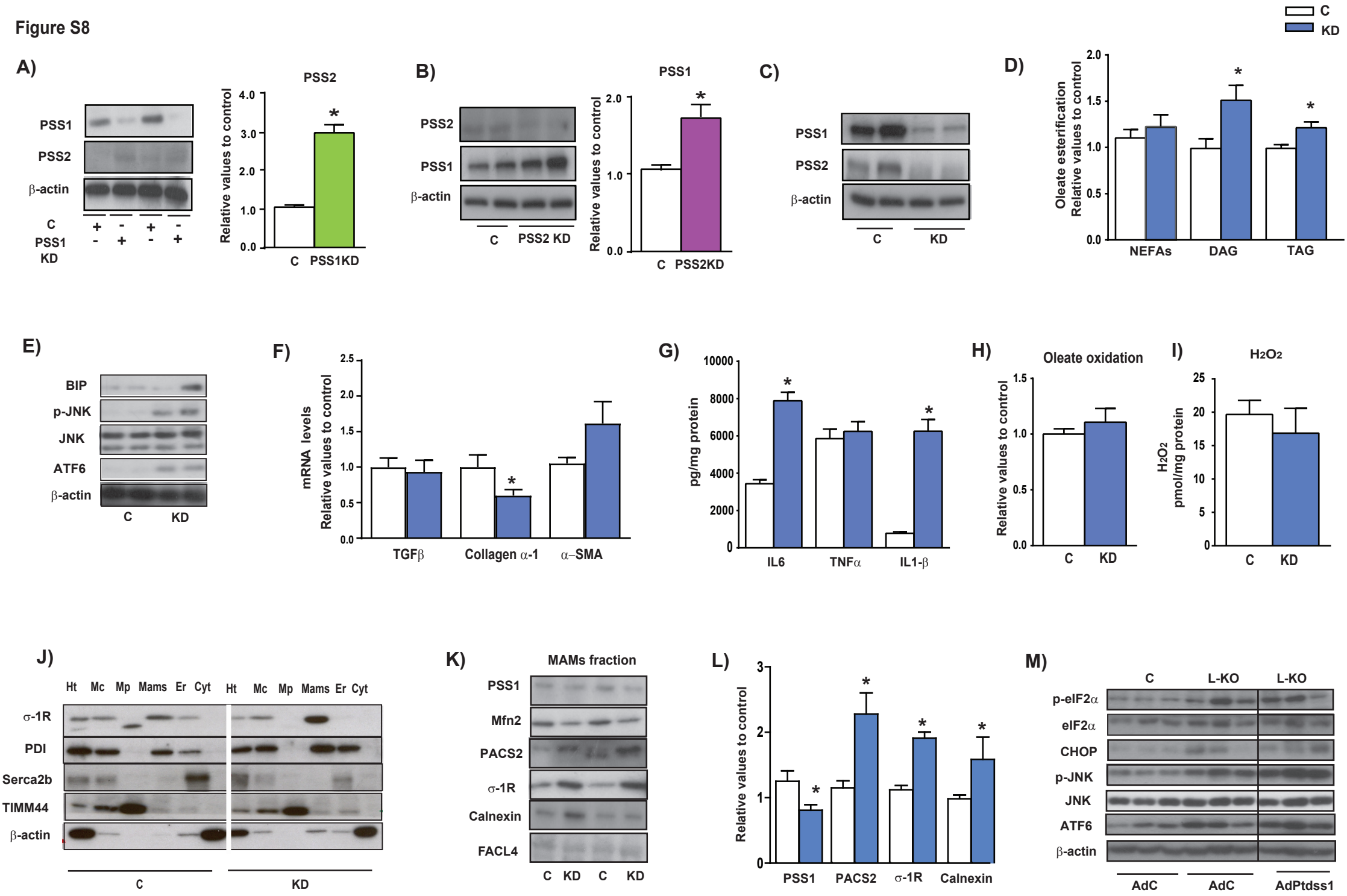
C
KD
A)
PSS1
PSS2
β-actin
C
PSS1 KD
PSS2
Relative values to control
C PSS1KD
B)
PSS2
PSS1
β-actin
C PSS2 KD
PSS1
Relative values to control
C PSS2KD
C)
PSS1
PSS2
β-actin
C KD
D)
Oleate esterification
Relative values to control
NEFAs DAG TAG
E)
BIP
p-JNK
JNK
ATF6
β-actin
C KD
F)
mRNA levels
Relative values to control
TGFβ Collagen α-1 α–SMA
G)
pg/mg protein
IL6 TNFα IL1-β
H)
Oleate oxidation
Relative values to control
C KD
I)
H2O2
H2O2
pmol/mg protein
C KD
J)
Ht Mc Mp Mams Er Cyt Ht Mc Mp Mams Er Cyt
σ-1R
PDI
Serca2b
TIMM44
β-actin
C KD
K)
MAMs fraction
PSS1
Mfn2
PACS2
σ-1R
Calnexin
FACL4
C KD C KD
L)
Relative values to control
PSS1 PACS2 σ-1R Calnexin
M)
C L-KO L-KO
p-eIF2α
eIF2α
CHOP
p-JNK
JNK
ATF6
β-actin
AdC AdC AdPtdss1

FIGURE S8. Effects of hepatic deficiency of phosphatidylserine synthase 1 and 2. A) Representative western blot of PSS1 and PSS2 protein and PSS2 protein quantification in 8-week-old mice 5 days after tail vein injection with control LacZ (C) or Ptdss1 siRNA adenoviruses (PSS1KD) (n=4 mice per group). B) Representative western blot of PSS1 and PSS2 protein levels and PSS1 quantification in mice 5 days after tail vein injection with control LacZ (C) or Ptdss2 siRNA adenoviruses (PSS2KD) (n=4 mice per group). C) Hepatic expression of PSS1 and PSS2 protein in control mice 5 days after tail vein injection with control LacZ (C) or Ptdss1/Ptdss2 siRNA adenoviruses (KD) (n=4 mice per group). D) Oleate incorporation into lipid species in isolated hepatocytes from C (open bars) and KD (blue bars) mice (n=4 mice per group). E) Western blot of hepatic ER stress protein markers in C and KD mice (n=4 mice per group). F) mRNA expression of hepatic fibrosis markers in C and KD mice (n=4 mice per group). G) Hepatic levels of pro-inflammatory factors in C and KD mice measured by ELISA (n=4 mice per group). H) Oleate oxidation in isolated hepatocytes from C and KD mice (n=4, each experiment performed in triplicate). I) Hepatic H_2O_2 levels in C and KD mice (n=4 mice per group). J) Quality control of the subcellular fractionation of liver obtained from C and KD mice. K–L) Representative western blot and quantification of protein markers in MAM fractions obtained from C and KD mice. M) Representative western blot of hepatic ER stress protein markers from control mice injected with lacZ adenoviruses (C+AdC), and L-KO mice injected either with lacZ (L-KO+AdC, red bars), or Ptdss1 adenoviruses (L-KO+AdPtdss1, blue bars) (n=3–5 mice per group). Data are expressed as mean ± SE. *$p<0.05$ vs. C.

Figure S9

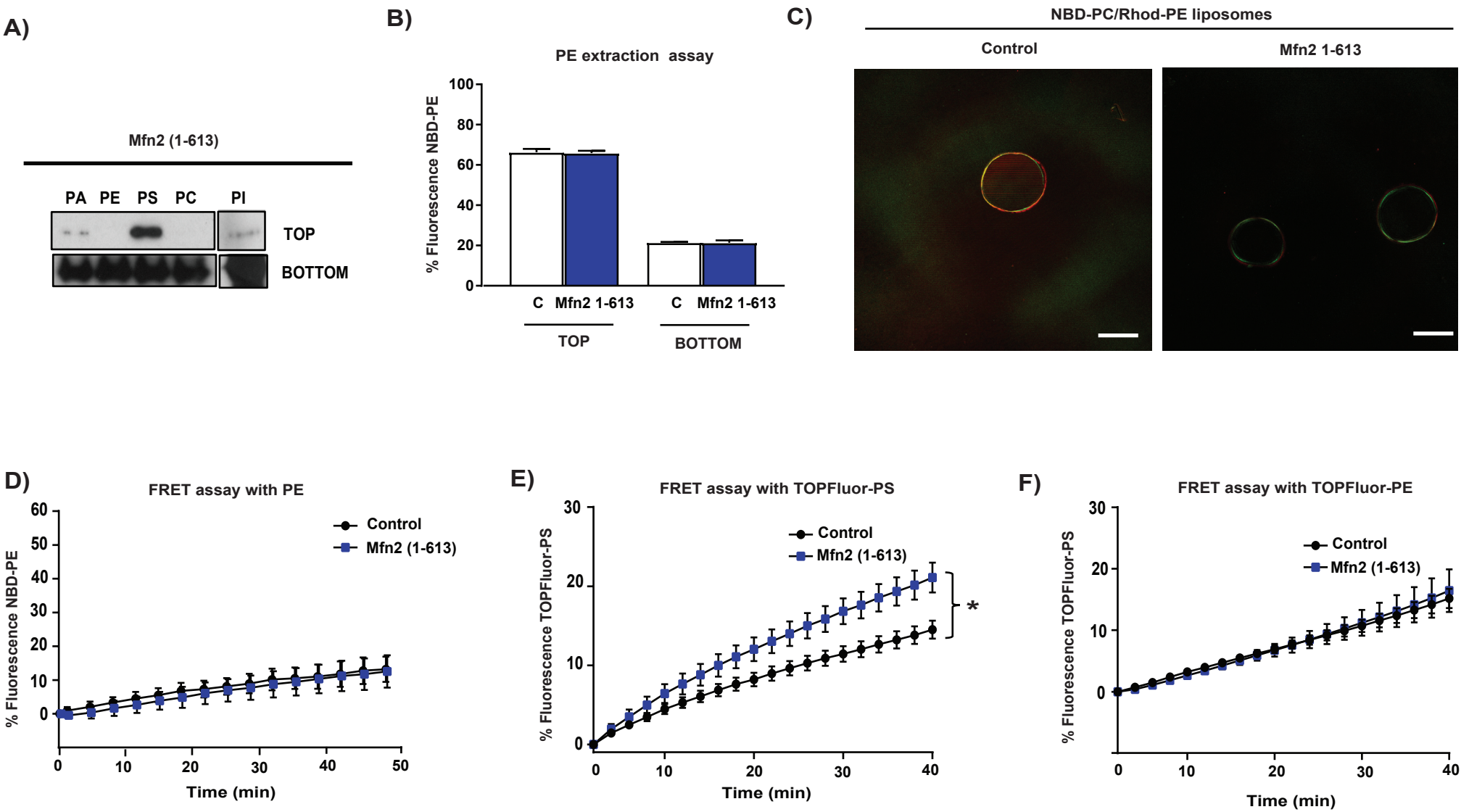
A)
Mfn2 (1-613)
PA PE PS PC PI
TOP
BOTTOM
B)
PE extraction assay
% Fluorescence NBD-PE
100
80
60
40
20
0
C Mfn2 1-613 C Mfn2 1-613
TOP
BOTTOM
C)
NBD-PC/Rhod-PE liposomes
Control
Mfn2 1-613
D)
FRET assay with PE
% Fluorescence NBD-PE
Control
Mfn2 (1-613)
Time (min)
E)
FRET assay with TOPFluor-PS
% Fluorescence TOPFluor-PS
Control
Mfn2 (1-613)
*
Time (min)
F)
FRET assay with TOPFluor-PE
% Fluorescence TOPFluor-PS
Control
Mfn2 (1-613)
Time (min)

FIGURE S9. Mfn2 specifically extracts PS from membranes. A) Representative western blot against histidine showing Mfn2 (1–613) after the liposome flotation assay with different non-fluorescent phospholipids using Mfn2 (1–613) purified from *E. coli*. B) Quantification of NBD-PE liposome extraction assay with Mfn2 (1–613) expressed in *E. coli* (n=3). C) Confocal microscopy images of NBD-PC/Rhod-PE liposomes in the absence or presence of Mfn2 (1–613). D) Kinetic FRET assay with NBD-PE and Rhod-PE to evaluate the capacity of Mfn2 (1–613) to dequench NBD-PE from liposomes (n=6). E) Kinetic FRET assay with TOPFluor-PS and doxyl-PC to evaluate the capacity of Mfn2 (1–613) to dequench TOPFluor-PS from liposomes (n=4). F) Kinetic FRET assay with TOPFluor-PE and doxyl-PC to evaluate the capacity of Mfn2 (1–613) to dequench TOPFluor-PE from liposomes (n=4). Data are expressed as mean ± SE. Statistical analysis in panels D, E and F was performed by using a two-way ANOVA. *$p<0.0001$ vs Control group.

Figure S10

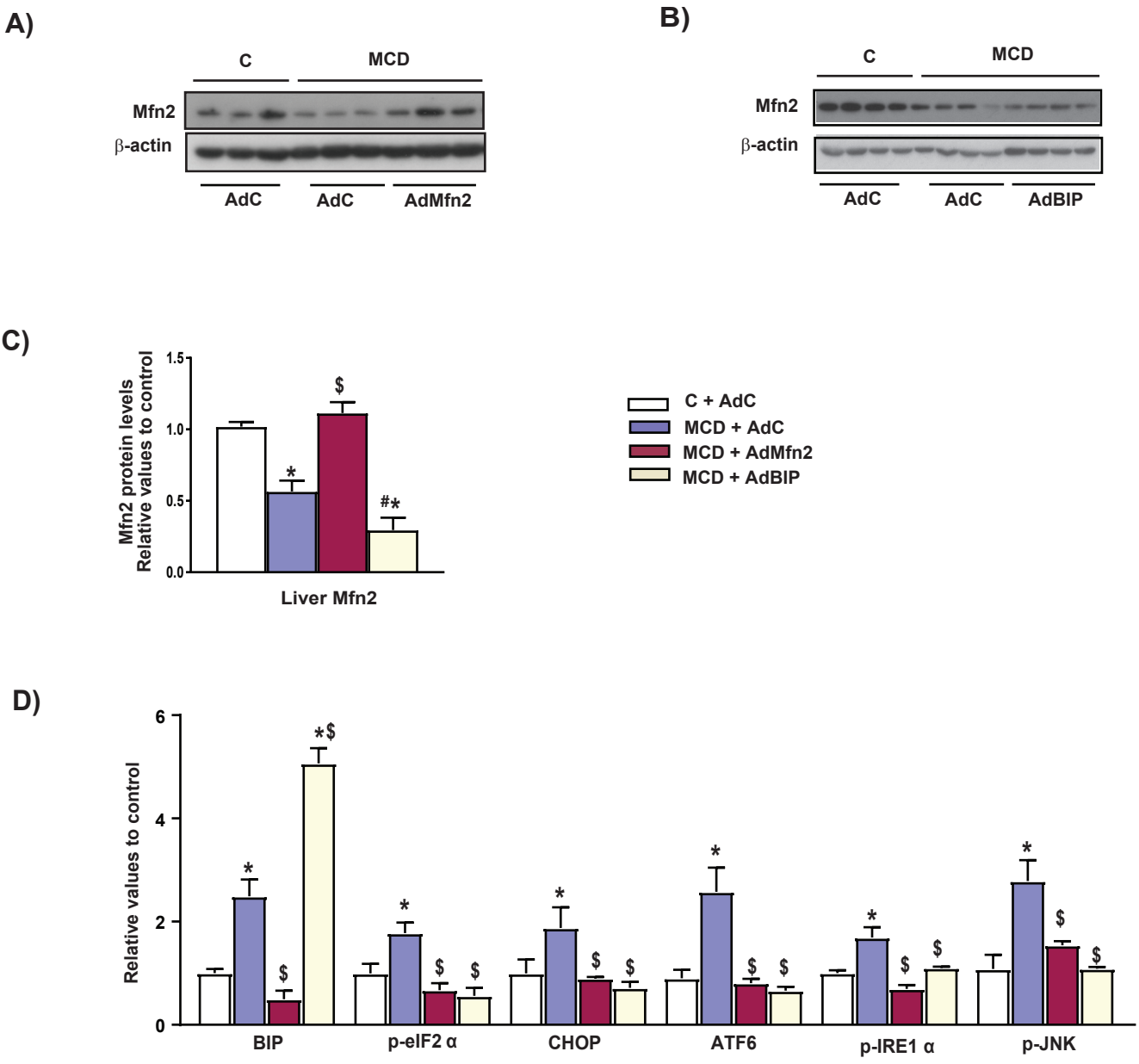
A)
C
MCD
Mfn2
β-actin
AdC
AdC
AdMfn2
B)
C
MCD
Mfn2
β-actin
AdC
AdC
AdBIP
C)
Mfn2 protein levels
Relative values to control
1.5
1.0
0.5
0.0
*
$
#*
Liver Mfn2
C + AdC
MCD + AdC
MCD + AdMfn2
MCD + AdBIP
D)
Relative values to control
6
4
2
0
BIP
p-eIF2 α
CHOP
ATF6
p-IRE1 α
p-JNK

FIGURE S10. Mfn2 re-expression improves the phenotype in a NASH mouse model. A) Western blot showing re-expression of Mfn2 in mice on chow diet (C) and methionine/choline-deficient diet combined with high-fat diet and supplemented with 0.1% L-methionine in drinking water (MCD) (n=4 mice per group). B) Western blot of BIP overexpression in C and MCD mice (n=4 mice per group). C) Quantification of Mfn2 protein in liver from control mice injected with AdC (null adenovirus) (C+AdC, white bars), MCD mice injected with AdC (MCD+AdC, blue bars), AdMfn2 (MCD+AdMfn2, red bars) or AdBIP (MCD+BIP, yellow bars) (n=4 mice per group). D) Quantification of hepatic ER stress protein markers from C+AdC, MCD+AdC, MCD+AdMfn2 and MCD+AdBIP mice. Data are expressed as mean ± SE. Statistical analysis was performed by using one-way ANOVA followed by post-hoc t tests. *$p<0.05$ vs. C+AdC, $^{\$}p<0.05$ vs. MCD+AdC and # $p<0.05$ vs. MCD+AdBIP.

Supplementary Methods.

Human liver biopsies

Liver biopsies were obtained from NAFLD patients undergoing bariatric surgery; liver biopsies from normal individuals were not collected due to ethical issues. Biopsies were processed conventionally for diagnostic purposes, histological grading, and staging, as described previously (Ferreira et al., 2011). In particular, all liver specimens were evaluated by an experienced pathologist, blinded to clinical data, and following the NAFLD histology scoring system. The severity of steatosis was graded from 0 to 3, inflammation from 0 to 3, hepatocellular ballooning from none to many, and fibrosis from 0 to 4. Each liver specimen was assessed for the presence or absence of NASH by pattern recognition, and for NAFLD activity score (NAS score), defined as the sum of steatosis, inflammation and hepatocyte ballooning. Patients with a NAS score of $\geq$5 were considered as likely to have NASH (Kleiner et al., 2005; Neuschwander-Tetri and Caldwell, 2003).

All patients gave written informed consent. The study protocols conformed to the Ethical Guidelines of the 1975 Declaration of Helsinki, revised in 2000, as reflected in a priori approval by the Hospital de Santa Maria (Lisbon, Portugal), by the Hospital Sant Joan de Reus (Institutional Review Board, project code: INFLAMED/15-04-30/4prog7) and Human Ethics Committee.

Animal care, generation of animal models, and diet treatments

All animal work was approved and conducted according to guidelines established. This project has been assessed favourably by the Institutional Animal Care and Use Committee from Parc Cientific de Barcelona (IACUC-PCB) and the IACUC considers that the above-mentioned project complies with standard ethical regulations and meets the requirements of current applicable legislation (RD 53/2013 Council Directive; 2010/63/UE; Order 214/1997/GC). Control and KO mice were littermates. Mice were kept under a 12 h dark-light period and provided a standard chow-diet and water *ad libitum*. Eight-week-old C57Bl6/J males were fed a standard or a high-fat diet for 3 weeks (60% calories from fat, D12451 and D12492 from Research Diets, New Brunswick, USA). To MCD experiments: Eight-week-old C57Bl6/J males were fed a standard of methionine choline deficient diet combined with high fat diet (A06071305 MCD with 45% HFD from Research Diets) and supplemented with 0.1% L-methionine on drinking

water during 3 weeks. At the times indicated in the figure legends, mice were anesthetized using isoflurane and sacrificed by cervical dislocation. Tissues used for RNA purification, protein extraction or histology were prepared as published (Liesa et al., 2008; Soriano et al., 2006).

DEN treatment

To further characterize the protector effect of Mfn2 in liver, we assessed an acute treatment with a high dose of the carcinogen Diethylnitrosamine (DEN). Then, we treated 16 week-old control and L-KO mice for 48h with a single injection of DEN at 50 mg/kg. Liver sections from DEN-treated or untreated mice were stained with anti-Ki67 and anti-γH2AX as well as Hematoxilin and Eosin staining. DNA damage and compensatory proliferation were assessed by microscopy on paraffin-embedded sections (Herranz et al., 2010). In addition, to corroborate the susceptibility of Mfn2 ablation to develop liver cancer we used DEN combined with high fat diet (HFD) to induce liver cancer in mice (Herranz et al., 2010; Wu et al., 2010). To this end, 5 days-old mice were injected with a single dose of DEN (5 mg/kg) and put on HFD immediately after weaning. After 7 month of treatment the mice were sacrificed and tumors in each liver lobule were counted and measured with a caliper.

Plasma measurements. Plasma concentrations of insulin, NEFA, ketone bodies, triglycerides, cholesterol, IL6, TNFα and IL-1β (Abnova) were measured following the manufacturer's instructions.

Liver subcellular fractionation and MAM purification

Liver fractions were purified as previously described (Wieckowski, Giorgi et al. 2009; Tubbs 2014). Briefly, after homogenization of about 1 g of liver with a Teflon potter in Isolation Buffer (225 mM mannitol, 75 mM sucrose, 0.5% BSA, 0.5 mM EGTA and 30 mM Tris-HCl, pH7.4), cellular debris and nucleus were removed with two centrifugations at 740 x *g* for 5 min. A small volume of supernatant was taken, this was called the homogenate fraction. Crude mitochondria were collected by centrifugation at 9,000 x *g* for 10 min, and the pellet was resuspended in Mitochondria Buffer (MB) (250 mM mannitol, 5 mM HEPES and 0.5 mM EGTA, pH 7.4). The supernatant was conserved for ER purification. Pure mitochondria and MAM fractions were obtained from the crude

mitochondria fraction with a Percoll medium centrifugation at 95,000x *g* for 30 min in a SW40 rotor (Beckman). Pure mitochondria (pM) at the bottom of the tube were collected, washed twice by centrifugation at 6,300 x *g* for 10 min, and resuspended in RIPA buffer. MAMs were collected from a white band in the middle of the tube. They were then diluted in MB and centrifuged at 6,300 x *g* for 10 min to remove mitochondrial contamination, pelleted with a 1-h centrifugation at 100,000 x *g* in a 70Ti rotor (Beckman), and finally resuspended in MB. The ER was purified by two centrifugations at 20,000 x *g* and 100,000 x *g* for 30 min and 1 h respectively. Finally, the ER pellet was washed once in MB with a 10 min centrifugation at 9,000 x *g* and resuspended in RIPA buffer. In order to estimate the amount of each fraction within the liver, proteins were determined using the PierceTM BCA Protein Assay kit (Thermo scientific). Purification yield was expressed as mg of protein/g of liver and the amount of MAM was then normalized by the amount of pure mitochondrial (pM) protein.

Hepatocyte isolation

Collagenase perfusion was used to isolate hepatocytes from male control and liver-specific Mfn2 knockout mice (25–28 g), as described (Massague and Guinovart, 1977). Cells were suspended in Dulbecco's Modified Eagle's Medium (DMEM), supplemented with 10 mM glucose, 10% (v/v) fetal bovine serum (FBS), 100 nM insulin (Sigma), and 100 nM dexamethasone (Sigma), and then seeded at a final density of 4×10^6 cells/cm^2 onto 60-mm diameter plastic plates treated with 0.001% (w/v) collagen solution (Sigma). Media were replaced with fresh M99 media-free serum, 1% BSA, and cells were incubated for 12–14 h.

Adenoviral transduction

The following adenoviruses were used in this study: Ad-LacZ, Ad-Mfn2Δ-Histidine (encoding for a truncated form of Mfn2= Mfn2 (1-613)) (Pich et al., 2005; Segalés et al., 2013). Ad-Mfn2 was cloned by recombination into the pAdeno-CMV-V5 adenoviral vector (Invitrogen) using the Gateway system. Adenoviruses were generated by transfection of the adenoviral expression vectors in human embryonic kidney cell line (HEK 293). The adenoviruses generated were then amplified at the *Unitat de Producció de Vectors Virals*-CBATEG (*Universitat Autònoma de Barcelona*). Ad-Ptdss1, Ad-Ptdss2 shRNAs and Ad. Ptdss1 (Vector Biolabs), AdControl and AdLinker (a gift from

Dr. Gokan Hotamisligil, Harvard University), and Ad-BIP (a gift from Dr. Jennifer Rieusset, INSERM Lyon) were also used.

Cells: Isolated hepatocytes were grown in DMEM 10% FBS. On the day of the experiment, they were infected at a multiplicity of infection (moi) of 50 pfu/cell, and all the experiments were performed 48 h after infection. After infection, cells were incubated for a further 16 h in infection medium before performing the experiment.

Animals: Adenovirus transductions of mice were performed between 8 and 10 weeks of age, and 1×10^9 IFU/mouse were injected via the tail vein. Livers were isolated after 5 days of adenovirus infection.

Oleate β-oxidation in isolated hepatocytes

Isolated hepatocytes were pre-incubated for 30 min at 37°C in 2 ml of *Krebs-Ringer bicarbonate Hepes* buffer containing 2% bovine serum albumin (fatty acid free-BSA; Sigma, St Louis, MO, USA) and 5 mmol/l glucose (incubation medium). The medium was gassed continuously with 95% O_2, 5% CO_2. The medium was then removed and replaced by 2 ml of fresh incubation medium, containing 1 μCi/ml D-[U]-^{14}C-Oleate (Amersham Biosciences). The hepatocytes were incubated for 180 min at 37°C. The test plates were hermetically sealed with parafilm with a centre well that contained a piece of filter paper saturated with 200 μl of 1M KOH (Sebastián et al., 2007). At the end of the incubation, the medium was acidified with 0.3 ml of 0.5N H_2SO_4 and gaseous $^{14}CO_2$ released after the acidification was trapped in the filter paper. The vials were incubated at 37°C for 60 min, and the filter papers were removed and transferred to vials for liquid scintillation counting (Sebastián et al., 2007).

Oleate incorporation into lipids in isolated hepatocytes

Isolated hepatocytes were pre-incubated for 30 min at 37°C in 2 ml of *Krebs-Ringer bicarbonate Hepes* buffer containing 2% bovine serum albumin (fatty acid free-BSA; Sigma, St Louis, MO, USA) and 5 mmol/l glucose (incubation medium). The medium was gassed continuously with 95% O_2, 5% CO_2. The medium was then removed and replaced by 2 ml of fresh incubation medium, containing 1 μCi/ml D-[U]-^{14}C-Oleate (Amersham Biosciences). The hepatocytes were incubated for 16 h at 37°C (95% O_2, 5% CO_2). At the end of the incubation, the medium was removed and plates were washed 3 times PBS 1X. Lipids were extracted and resolved in a thin layer chromatograph as reported (Sebastián et al., 2007).

Histological sample preparation and analysis

For light microscopy, sections were stained with hematoxylin and eosin. For neutral lipids, liver slices were stained with Oil Red O following Roy Ellis (Woodville, South Australia). For the preparation of livers for electron microscopy, samples were sectioned in small fragments with a razor blade to 1 mm and then fixed in 2.5% glutaraldehyde 2% paraformaldehyde solution 0.1 M at 4 C for 2 h. The samples were washed three times with 0.1 M phosphate buffer. Following post-fixation in 1% osmium tetroxide in 0.1 M phosphate buffer at 4ºC for 2 h, they were then washed with highly pure water and kept overnight in 0.1 M phosphate buffer. Afterwards, samples were dehydrated at 4ºC under shaking in graded solutions of acetone (50%, 70% and 90%) in highly pure water. They were then gradually infiltrated with Eponate 12 Resin (TED PELLA 18010), and polymerization of the resin was processed for 48 h at 60ºC. Thin sections (50-nm) were cut using a Leica EM UC6 (Leica, Vienna) and mounted on bare 200-mesh copper grids. Sections were stained with uranyl acetate 2% for 30 min, then washed with highly pure water and finally incubated for 5 min with lead citrate and air-dried. Soleus samples were prepared at equal lengths along the long axis of the muscle. Sample sections were viewed on an FEI CM-12 transmission electron microscope.

Western blotting and immunoprecipitation assays

Homogenates for Western blot analyses were obtained from either cell cultures or tissues. Cells were collected in ice-cold PBS 1X and homogenized with a douncer in lysis buffer (50 mM Tris pH 7.5, 150 mM NaCl, 1% Triton X-100, 2 mM EDTA, 2 mM sodium ortovanadate, 50 mM NaF, 20 mM sodium pyrophosphate and protease inhibitors cocktail tablet, Roche) and centrifuged at 700 x *g* for 10 min to remove nuclei, cell debris, and floating cells. Tissues samples were homogenized in 10 volumes of lysis buffer using a polytron. Homogenates were rotated for 1 h at 4ºC in an orbital shaker and centrifuged at 13,000 rpm for 15 min at 4ºC. Proteins from total homogenates were resolved in 10% or 15% acrylamide gels for SDS-PAGE and transferred to Immobilon membranes (Millipore). The following antibodies were used: Mfn2, p-IRE1 and IRE1(1/1000, Abcam), p-eIF2α, eIF2α, BiP, p-PERK, PERK, pJNK, JNK (1/1000, Cell Signaling), CHOP, Ptdss1 and Ptdss2 (1/1000, Santa Cruz), ATF6 (1/1000, Imgenex), β-actin (1/10000, Sigma), α-tubulin (1/8000, Sigma), and porin (1/5000, Calbiochem). Proteins

were detected by the ECL method (Enrique-Tarancon et al., 2000) and quantified by scanning densitometry.

RNA extraction and real-time PCR

Mice were killed by cervical dislocation, and tissues were immediately frozen for RNA isolation. RNA from liver tissues was extracted using a protocol combining TRIzol reagent (Invitrogen, Carlsbad Ca, USA) and RNAeasy® minikit columns (Qiagen, Alameda, CA, USA), following the manufacturer's instructions. RNA was reverse-transcribed with the SuperScript RTIII kit (Invitrogen, Carlsbad Ca, USA). PCRs were performed using the ABI Prism 7900 HT real-time PCR machine (Applied Biosystems, USA) and the SYBR® Green PCR Master Mix or the Taqman Probes 20X (Applied Biosystems, USA). All measurements were normalized to β-actin and GAPDH.

Hepatic triglyceride measurements

Levels of mouse liver triglycerides were quantified using the Triglyceride Determination Kit TRO100 with appropriate standards (Sigma-Aldrich, St. Louis, MO). Frozen liver samples were weighed, put into 2 ml of a chloroform:methanol mixture (2:1, v/v), and incubated for 2 h at room temperature with occasional shaking. Following the addition of 0.2 volumes of water, vortexing, and centrifuging at 2,500 x *g*, the lower phase containing the lipids was collected and dried under vacuum in a rotary evaporator for 5–6 h. The dried pellets were resuspended in the reaction buffer provided in the kit. Results were expressed as mg/g tissue.

Lipidomic analysis from liver

Lipidomic analysis was done as described previously (Kotronen et al., 2010; Nygren et al., 2011). Briefly, liver samples were cryo-homogenized (Covaris, CryoPrep CP02, MA) and weighed (5 mg). An aliquot (20 µL) of an internal standard mixture containing PC(17:0/0:0), PC(17:0/17:0), PE(17:0/17:0), PG(17:0/17:0)[rac], Cer(d18:1/17:0), PS(17:0/17:0), PA(17:0/17:0) (Avanti Polar Lipids, Alabaster, AL), MAG(17:0/0:0/0:0)[rac], DAG(17:0/17:0/0:0)[rac] and TAG(17:0/17:0/17:0) was added to the sample, and the lipids were extracted using a mixture of HPLC-grade chloroform and methanol (2:1; 400 µL). 50 µl of 0.9% NaCl was added, and the lower phase (200

µL) was collected and 20 µL of an internal standard mixture containing labeled PC (16:1/0:0-D_3), PC(16:1/16:1-D_6) and TAG(16:0/16:0/16:0-$^{13}C3$) was added.

Lipid extracts were analyzed on a Waters Q-Tof Premier mass spectrometer combined with an Acquity Ultra Performance LCTM (UPLC). The column (at 50°C) was an Acquity UPLC^{TM} BEH C18 1 × 50 mm with 1.7-µm particles. The solvent system included A. ultrapure water (1% 1 M NH4Ac, 0.1% HCOOH) and B. LC/MS grade acetonitrile/isopropanol (5:2, 1% 1M NH4Ac, 0.1% HCOOH). The gradient started from 65% A / 35% B, reached 100% B in 6 min and remained there for the next 7 min. The flow rate was 0.2 ml/min and the injected amount was 1.0 µl (Acquity Sample Organizer). Reserpine was used as the lock spray reference compound. The lipid profiling was carried out using ESI+ mode, and the data were collected at mass range of m/z 300–1200 with a scan duration of 0.2 sec. The data were processed using MZmine software version 6.0 (Katajamaa et al., 2006; Pluskal et al., 2010) and normalized using lipid class-specific internal standards. Lipid species identification was done using an internal spectral library or tandem mass spectrometry.

QTOF-based untargeted lipidomics of liver subcellular fractionation

For protein precipitation three volumes of acetone were added to each sample (containing 100 µg of protein). After acetone addition the samples were vortexed for 10 seconds, incubated at 4ºC for 30 min and centrifuged at 100g, at 4ºC for 10 minutes. Then, the supernatant was recovered and evaporated using a Speed Vac (Thermo Fisher Scientific, Barcelona, Spain).

After supernatant evaporation, 250 µl of methanol were added and vortexed for 10 s. Then, 500 µl of chloroform (containing internal standard) were added and vortexed for 10 s. Finally, 200 µl of KCl 0.7% were added and vortexed for 10 s and samples centrifuged at 1000 g at 4 °C for 15 min. The chloroform phase (lower) was recovered in a glass tube and aliquoted in chromatographic vials.

For LC-Q-TOF-based lipid molecular species analyses, lipid extracts were subjected to liquid chromatography-mass-spectrometry using a HPLC 1290 series coupled to ESI-Q-TOF MS/MS 6520 (Agilent Technologies, Barcelona, Spain) as previously described (Sandra et al.). Four microliters of lipid extract were injected onto an XBridge BEH C18 shield column (100 mmL × 2.1 mm ID × 1.7 µm; Waters, Milford, MA, USA) kept at

80 °C. The mobile phases, delivered at 0.5 ml/min, consisted of ammonium formate (20 mM at pH 5) (A) and methanol (B). The gradient started at 50% B and reached 70% B in 14 min and was followed by a slow gradient of 70–90% B over 50 min and an isocratic separation at 90% B for 15 min. The mobile phase B subsequently reached 100% over 5 min and was maintained for an additional 5 min. Data were collected in positive electrospray ionization-TOF operated in full-scan mode at 100–3000 m/z in an extended dynamic range (2 GHz) (MassHunter Data Adquisition Sofware, Agilent Technologies, Barcelona, Spain), using N2 as nebulizer gas (5 L/min, 300 °C). The capillary voltage was 3500 V with a scan rate of 1 scan/s.

MassHunter Qualitative Analysis Software (Agilent Technologies, Barcelona, Spain) to obtain the molecular features of the samples, representing different, co-migrating ionic species of a given molecular entity using the Molecular Feature Extractor (MFE) algorithm (Agilent Technologies, Barcelona, Spain) (Jové et al., 2013). MassHunter Mass Profiler Professional Software (Agilent Technologies, Barcelona, Spain) and Metabolanalyst Software (Xia et al. 2016; Chong et al., 2018) was used to perform a non-targeted lipidomic analysis over the extracted features. Only those features with a minimum abundance of 5000 counts and 2 ions as a minimum were selected. After that, the molecular characteristics in the samples were aligned using a retention time window of 0,1% ± 0,25 min and 20,0 ppm ± 2,0 mDa. Quality control-based correction was performed in order to correct the sample intensities according to injection order. A LOESS regression was performed for each QC metabolite, using polynomials of second degree and with an optimum smoothing parameter each time. Sample values were predicted and the relation between real values and predicted values was obtained, based on (Broadhurst et al. 2018; Dunn et al. 2011). To avoid background, only common features (found in at least 70% of the samples of the QC) were taken into account to correct for individual bias. Multivariate statistics (Partial Least Squares Discriminant Analysis (PLS-DA) and Hierarchical Analyses) were done using Metaboanalyst software (Xia et al. 2016; Chong et al., 2018). Variable importance in projection (VIP) score was calculated using Metaboanalyst software [72, 73]. The masses with an important weight defining PLS-DA model and Hierarchical analyses as well as those masses representing significant differences by Student T-Test ($p < 0.05$), defined by exact mass and retention time, were searched against the LIPID MAPS database (accuracy < 20 ppm) (Fahy et al., 2007). The identities obtained were compared to retention time of the authentic standards

added. Finally, identities were confirmed by MS/MS by checking the MS/MS spectrums using LipidBlast software (Kind et al., 2013) and LipidMatch, a R-based tool for lipid identification (Koelmel et al., 2016).

^{3}H- L-serine incorporation into phospholipids in subcellular fractions

Liver was homogenized (use Teflon-glass homogenizer) in Isolation Buffer (225mM Mannitol, 25mM Hepes-KOH, 1mM EGTA, pH7.4 add protease inhibitors tripsins and chimotripsins) at a ratio of 4 ml of IB for every gram of tissue. The homogenate was pelleted for 10 min at 1,500 x *g* at 4°C. SPN was transferred to a new tube and pelleted again under the same conditions. SPN was transferred again to a new tube and pelleted at 13,000 x *g* for 20 min at 4^{0}C. This new pellet contained the crude mitochondrial fraction and was used to measure lipid transfer because it contains mitochondria and ER-MAM. The SPN contained the ER fraction, which was pelleted at 100,000 x *g* for 1 h at 4^{0}C. This pellet was used as a control in the assay. 1 mg of the fraction was pelleted again and resuspended in 200 µl of Ptdser assay buffer (25 mM Hepes-KOH, 10 mM $CaCl_2$ adding 0.4 mM of ^{3}Hser (20–30 µci/umol) pH 7.4). The mixture was incubated for 45 min at 37ºC and the reaction was stopped by adding 3 volumes of chloroform: MeOH (2:1). The lipids were extracted using the Folch Method, dried by N_2, and run in a TLC as reported (Area-Gomez, 2014; Area-Gomez et al., 2012).

Mfn2 imunoprecipitation for phospholipid binding assays

Liver from control mice was homogenized in 50 mM Tris-HCl (pH 7.4), 150 mM NaCl, 1 mM EDTA, 1% Triton X-100, 2 mM sodium ortovanadate, 50 mM NaF, 20 mM sodium pyrophosphate and 1% SDS, pH 7.4. Protease inhibitors: Pepstatin A 2 uM, Leupeptin 2 uM, PMSF 1 mM or one tablet from Roche per 10 ml of fresh buffer added. These conditions cause dissociation of Mfn2 from other potential binding partners including lipid species.

The lysate was centrifuged for 10 min at 10,000 x *g* at 4ºC. The supernatant was warmed at 95ºC for 5 min. Supernatant was diluted 10 times with homogenization buffer without SDS and placed onto 50% Protein G-Agarose beads (30ul). 10 ul of Mfn2 ab or IgG was added and the mixture was incubated O/N at 4ºC on the roller. Next day, washes were done with 300–500 ul washing buffer (5 times). Then protein was extracted using glycine buffer elution (0.2 M glycine pH 2.0–3.0) and neutralized with Tris, pH 8.0. Protein

concentration was determined by the BCA Pierce assay, and the protein was used in fresh to assay the lipid strips. A small aliquot of protein was used for Western blotting.

Purification of a short Mfn2 (1-613) for phospholipid binding assays

Liver Mfn2 KO mice were injected with $1X10^9$ pfu/bodyweight Ad-Mfn2Δ-Histidine through the tail vein; the adenovirus was used as previously reported (Segalés et al., 2013). Injected mice were left in *ad libitum* conditions for adenoviral expression. After 5 days mice were sacrificed and liver was extracted and immediately frozen in liquid nitrogen and stored at -80ºC until the assay was performed. Liver was homogenized in lysis buffer (25 mM Imidazol, 300 mM NaCl, 1% Triton X-100, 100 mM $NaPO_4$, 1 mM Na_3VO_4, 50 nM calyculin A and EDTA-free complete pH 7.5 and 1% SDS) and put to rotate for 1 h at 4ºC. The lysate was centrifuged at 10,000 x *g* for 10 min at 4ºC. Then the supernatant was warmed to 95ºC for 5 min. The supernatant was then diluted ten times with lysis buffer and incubated with Ni-NTA beads (previously equilibrated with lysis buffer without SDS). The mixture was incubated O/N at 4ºC under rotation. Next day, the beads were washed 5 times with washing buffer (50 mM Imidazol, 500 mM NaCl and 1 mM Na_3VO_4, pH 7.5). At the end elution buffer (250 mM Imidazol, 300 mM NaCl, pH 7.5) was added and the mixture was put into the thermomixer for 15 min at 25ºC and 1150 rpm. Protein concentration was determined by the BCA Pierce assay, and the protein was used in fresh to assay the lipid strips. A small aliquot of protein was used for Western blotting.

Purification of Mfn2 (1-613), Mfn1(1-592) and Mfn2(21-613) expressed in *E.coli*.

100ng of cut vector pOPINI and 100ng of insert were used to clone the Mfn2(1-613) or Mfn1(1-592) or Mfn2(21-613) form by InFusion, according to manufacturer's instructions. For all constructs the plasmids were transformed in Rosetta cells. Briefly, transform 5ul of each infusion reaction, and the equivalent amount of the controls. Plate 100ul of settled cells,cb+iptg+xgal antibiotics, and leave ON at 37ºC. Lysis Buffer: 1% SDS +300mM NaCl+20mM Imidazole+1mM NaVO4+1.4mM KCl. Wash Buffer: 500mM NaCl+40mM Imidazole. Elution Buffer: 300mM NaCl+250mM Imidazole. Each 2ml pellet was resuspended in 200ul of Lysis Buffer then sonicated for 2x10'' at 20%. The homogenate was incubated in an ice-water bath 30'. Spin 20' at 20000g at 4ºC. SN was transferred to a new tube CRX (200ul). To magnetic niquel beads: Bind 2 * 100ul samples to 20ul of beads each, 30' shaking at RTº. Bind beads to the magnets, and recover

flow through samples. Add 100ul of each Wash Buffer to the beads, bind for 5' shaking at RT. Bind beads to the magnets and collect Washes 1. Repeat this wash again, and collect Washes 2. Add 50ul of Elution Buffer to the beads, bind for 5' shaking at RT. Bind beads to the magnets and collect Elution1 samples. Bind beads to the magnets and collect Elution2 samples.

Binding to Lipid Strip assays

Membrane lipid strips™ were obtained from Echelon Bioscience (P-6002 and P-6003). Lipid strips were assayed, following the manufacturer's instructions. Briefly, the membrane was blocked with 3% of fatty acid-free BSA in TBS-Tween 0.1% and gently agitate O/N at 4ºC. After discarding the blocking solution, the membrane was incubated with 10 µg/ml of protein at room temperature for 1 h. The protein solution was discarded, and the membrane washed for about 8 min with TBS-Tween 0.1% (repeated this step 4–5 times). The membrane was then incubated with a 1:1,000 dilution of primary antibody in 3% of fatty acid-free BSA TBS-Tween 0.1%. Gently agitated for 1 h at RT. The antibody solution was discarded, and the membrane washed for about 8 min with TBS-Tween 0.1% (repeated this step 4–5 times). The membrane was incubated with a 1:25,000 dilution of secondary antibody in 3% of fatty acid-free BSA TBS-Tween 0.1%. Gently agitated for 1 h at RT. The secondary antibody solution was discarded, and the membrane washed for about 8 min with TBS-Tween 0.1% (repeated this step 4–5 times). The bound of protein to lipid was detected by Chemiluminescent or ECL.

Lipid binding by liposome flotation assays

Phospholipids and *E. coli* lipids were obtained from Avanti Polar Lipids, unless is stated. Lipids in stock solution in chloroform were prepared at 1 mM concentration (according to https://bio-protocol.org/e2169 and (Apellániz and Nieva, 2015)): 80% of: *E. coli* (100500P) or PC (860355P) and 20% of: PC (860355P), PS (840037P), PA (830855P), PE (850705P) or PI (P2517-25MG). The lipid suspension was incubated at room temperature for 1 hour. Then, it was first sonicated during 4 cycles of 3 minutes each (Ultrasonic Cleaner; Branson 200) and then 5 freeze/thaw cycles in liquid nitrogen/warm water (26ºC) were performed to break the lipid cake. Finally the liposome mix was extruded through 400 nm polycarbonate membrane filter using a mini-extruder for large unilamellar vesicles (LUVs) formation.

Five µl of protein (≈1.5µM) were incubated with 45 µl of *E. coli* or PC liposomes containing either PA, PE, PC, PS or PI in TBS 1X during 1 hour at room temperature as reported. After the incubation, the mixture was subjected to liposome flotation. Briefly, the 50 µl of liposome/protein mixture was put into 800 µl of an ultracentrifuge tube (Beckman Coulter, ref: 343776) and mixed with 120 µl of TBS 1X containing 60% sucrose (Sigma). The mixture was subsequently overlaid by 200 µl of TBS 1X containing 27% sucrose and then by 150 µl of TBS 1X containing 17% sucrose. After centrifugation at 84000 rpm for 3h at 4ºC, fractions were collected from top to bottom with a Hamilton syringe, and each fraction was analyzed by western blotting as reported (Apellániz and Nieva, 2015).

Lipid extraction assay

To monitor PS transfer extraction from liposomes we followed the protocol proposed by Kawano et. al.(Kawano et al., 2018; Krick et al., 2012). 200 µM liposomes: 80% of PC (860355P) and 20% of NBD-PS (810193P) or NBD-PE (810154P), were hydrated in TBS 1X (50 mM Tris-Cl, pH 7.5, 150 mM NaCl). The lipid suspension was incubated at room temperature for 1 hours. Then, it was first sonicated during 4 cycles of 3 minutes each (Ultrasonic Cleaner; Branson 200) and then 5 freeze/thaw cycles in liquid nitrogen/warm water (26ºC) were performed to break the lipid cake. Finally the liposome mix was extruded through 400 nm polycarbonate membrane filter using a mini-extruder for large unilamellar vesicles (LUVs) formation. For lipid extraction, 10 µl of protein (≈3 µM) of protein were mixed with 90 µl of liposomes in 100µl TBS 1X and incubated at room temperature for 3 hours. After the incubation, the mixture was subjected to liposome flotation. The mixture of liposome/protein in TBS 1X was put into 5 ml of an ultracentrifuge tube (Beckman Coulter, ref: 344057) and mixed with 1400 µl of buffer A (20mM Tris-HCl, pH 7.4, and 150mM NaCl) and 1500 µl of buffer A containing 80% Nycodenz AG (Axis-Shield). The mixture was subsequently overlaid by 1500 µl of buffer A containing 30% Nycodenz AG and then 900 µl of buffer A without Nycodenz AG (see figure 4A). After centrifugation at 54000 rpm for 2h at 4ºC, 2 different fractions, top and bottom, were collected and analyzed for fluorescence with Spectra fluorimeter (SYNERGY H1M Fluorescence plate reader) at excitation/emission 460-590nm and protein quantification by western blot.

***In vitro* phospholipid FRET assays**

To monitor the kinetics of FRET reaction, we assessed a modified protocol reported by Potting et. al. and Connerth et al. (Connerth et al., 2012; Potting et al., 2013). Briefly, Donor liposomes (12,5 µM): 90% *E. coli* (100500P), 2% Rhod PE (810158P), 8% NBD-PE (810154P) or NBD-PS (810193P) or NBD-PA (810174P) or NBD-PC (810131P) were resuspended in BLTS (10% sucrose in buffer BLT= 5mM Tris/HCl ph 7.4, 150mM NaCl), and acceptor liposomes (50µM): 90% E. coli (100500P) and 10% of PC (860355P) or PS (840037P) or PA (830855P) or PE (850705P) were resuspended in BLT buffer without sucrose. The lipid suspension was incubated at room temperature for 1 hour. Then, it was first sonicated during 4 cycles of 3 minutes each (Ultrasonic Cleaner; Branson 200) and then 5 freeze/thaw cycles in liquid nitrogen/warm water (26ºC) were performed to break the lipid cake. Finally the liposome mix was extruded through 400 nm polycarbonate membrane filter using a mini-extruder for large unilamellar vesicles (LUVs) formation. The donor and acceptor liposomes were mix with 200nM of purified recombinant protein and fluorescence of NBD was monitored during 3 hours in TECAN SAFIRE II-BASIC at constant temperature of 25C.

To TOPFluor liposomes: 12,5 µM Donor liposomes contained: 90% *E. coli* (100500P), 2% Doxyl PC (810604P), 8% TopFluor PS (810283P), or TopFluor PE (810282P) were resuspended in BLTS and mixed with the same acceptor liposomes prepared for NBD liposomes. Next, exactly the same protocol above described for NBD to monitor kinetics was assessed.

Liposome imaging

Donor liposomes (12,5 µM): 90% *E. coli* (100500P), 2% Rhod PE (810158P), 8% NBD-PC (810131P) or NBD-PS (810193P) resuspended in BLTS and acceptor liposomes (50µM): 90% E. coli (100500P) and 10% of PC (860355P) or PS (840037P) resuspended in BLT were incubated with 200nM of recombinant Mfn2 (1-613) protein in 300 µl buffer TA (20 mM Tris/HCl pH 7.4, 150 mM NaCl, 1 mM EDTA) at 25°C. After incubation the mixture was placed on ice, mixed with 100 µl buffer TA30 (30% sucrose in TA) and incubated for 10 min. The mix was placed on an ultracentrifuge tube and overlaid with 600 µl buffer TA5 (5% sucrose in TA), 400 µl ofTA2.5 (2.5% sucrose in TA) and 75 µl

buffer TA. Tubes were centrifuged at 217,000 xg for 2.5 h. Fractions fraction of 750 µl from the top middle and bottom were collected to be analyzed (Connerth et al., 2012). Liposomes were identified by confocal following bibliographic examples of liposome imaging (Gabor, 2011; Ruozi et al., 2011). Confocal images were obtained with a spectral confocal microscope multiphoton (Leica, Mannheim, Germany) and a Leica confocal system equipped with a 3-channel multiband Leica scanner TCS SP5. To obtain confocal images a small drop of the extraction flotation assay sample (usually 5 µl) was transferred to a coverslip (slide) and directly observed. Samples were scanned using a 63z Leitz objective (oil) to analyze the liposomes using LAS AF software from Leica. The NBD was excited with the 488 laser.

Statistical Analysis

Phospholipid content measured by lipidomics was analyzed separately using a linear model in which type of sample (control or L-KO) and experimental batch were included as covariates. Values were previously Box-Cox transformed in order to fit the assumptions of the model. Adjusted mean groups and fold-changes were extracted from the models and presented in their original scale. Statistical significance was assessed using the corresponding F-test.

The rest of the data presented in this work was analyzed with Student's t test or ANOVA followed by post-hoc t tests. Data are presented as mean ± SEM unless stated. Significance was established at $P \leq 0.05$.

References.

Apellániz, B., and Nieva, J.L. (2015). Fusion-competent state induced by a C-terminal HIV-1 fusion peptide in cholesterol-rich membranes. Biochimica et Biophysica Acta (BBA) - Biomembranes *1848*, 1014-1022.

Area-Gomez, E. (2014). Chapter Eleven - Assessing the Function of Mitochondria-Associated ER Membranes. In Methods in Enzymology, N.M. Anne, and C.C. David, eds. (Academic Press), pp. 181-197.

Area-Gomez, E., del Carmen Lara Castillo, M., Tambini, M.D., Guardia-Laguarta, C., de Groof, A.J.C., Madra, M., Ikenouchi, J., Umeda, M., Bird, T.D., Sturley, S.L., *et al.* (2012). Upregulated function of mitochondria-associated ER membranes in Alzheimer disease, Vol 31.

Connerth, M., Tatsuta, T., Haag, M., Klecker, T., Westermann, B., and Langer, T. (2012). Intramitochondrial Transport of Phosphatidic Acid in Yeast by a Lipid Transfer Protein. Science *338*, 815-818.

Enrique-Tarancon, G., Castan, I., Morin, N., Marti, L., Abella, A., Camps, M., Casamitjana, R., Palacin, M., Testar, X., Degerman, E.*, et al.* (2000). Substrates of semicarbazide-sensitive amine oxidase co-operate with vanadate to stimulate tyrosine phosphorylation of insulin-receptor-substrate proteins, phosphoinositide 3-kinase activity and GLUT4 translocation in adipose cells 1. BiochemJ *350 Pt 1*, 171-180.

Ferreira, D.M.S., Castro, R.E., Machado, M.V., Evangelista, T., Silvestre, A., Costa, A., Coutinho, J., Carepa, F., Cortez-Pinto, H., and Rodrigues, C.M.P. (2011). Apoptosis and insulin resistance in liver and peripheral tissues of morbidly obese patients is associated with different stages of non-alcoholic fatty liver disease. Diabetologia *54*, 1788-1798.

Gabor, F. (2011). "Characterization of Nanoparticles Intended for Drug Delivery". Scientia Pharmaceutica *79*, 701-702.

Herranz, D., Munoz-Martin, M., Canamero, M., Mulero, F., Martinez-Pastor, B., Fernandez-Capetillo, O., and Serrano, M. (2010). Sirt1 improves healthy ageing and protects from metabolic syndrome-associated cancer. Nat Commun *1*, 3.

Katajamaa, M., Miettinen, J., and OreŠiČ, M. (2006). MZmine: toolbox for processing and visualization of mass spectrometry based molecular profile data. Bioinformatics.

Kawano, S., Tamura, Y., Kojima, R., Bala, S., Asai, E., Michel, A.H., Kornmann, B., Riezman, I., Riezman, H., Sakae, Y.*, et al.* (2018). Structure–function insights into direct lipid transfer between membranes by Mmm1–Mdm12 of ERMES. The Journal of Cell Biology *217*, 959-974.

Kleiner, D.E., Brunt, E.M., Van Natta, M., Behling, C., Contos, M.J., Cummings, O.W., Ferrell, L.D., Liu, Y.-C., Torbenson, M.S., Unalp-Arida, A.*, et al.* (2005). Design and validation of a histological scoring system for nonalcoholic fatty liver disease. Hepatology *41*, 1313-1321.

Kotronen, A., Seppänen-Laakso, T., Westerbacka, J., Kiviluoto, T., Arola, J., Ruskeepää, A.-L., Yki-Järvinen, H., and Orešič, M. (2010). Comparison of Lipid and Fatty Acid Composition of the Liver, Subcutaneous and Intra-abdominal Adipose Tissue, and Serum. Obesity *18*, 937-944.

Krick, R., Busse, R.A., Scacioc, A., Stephan, M., Janshoff, A., Thumm, M., and Kühnel, K. (2012). Structural and functional characterization of the two phosphoinositide binding sites of PROPPINs, a β-propeller protein family. Proceedings of the National Academy of Sciences *109*, E2042-E2049.

Liesa, M., Borda-d'Agua, B., Medina-Gomez, G., Lelliott, C.J., Paz, J.C., Rojo, M., Palacin, M., Vidal-Puig, A., and Zorzano, A. (2008). Mitochondrial fusion is increased by the nuclear coactivator PGC-1beta. PLoS ONE *3*, e3613.

Massague, J., and Guinovart, J.J. (1977). Insulin control of rat hepatocyte glycogen synthase and phosphorylase in the absence of glucose. FEBS Lett *82*, 317-320.

Neuschwander-Tetri, B.A., and Caldwell, S.H. (2003). Nonalcoholic steatohepatitis: Summary of an AASLD Single Topic Conference. Hepatology *37*, 1202-1219.

Nygren, H., Seppänen-Laakso, T., Castillo, S., Hyötyläinen, T., and Orešič, M. (2011). Liquid Chromatography-Mass Spectrometry (LC-MS)-Based Lipidomics for Studies of Body Fluids and Tissues. In Metabolic Profiling, T.O. Metz, ed. (Humana Press), pp. 247-257.

Pich, S., Bach, D., Briones, P., Liesa, M., Camps, M., Testar, X., Palacin, M., and Zorzano, A. (2005). The Charcot-Marie-Tooth type 2A gene product, Mfn2, up-regulates fuel oxidation through expression of OXPHOS system. HumMolGenet *14*, 1405-1415.

Pluskal, T., Castillo, S., Villar-Briones, A., and Oresic, M. (2010). MZmine 2: Modular framework for processing, visualizing, and analyzing mass spectrometry-based molecular profile data. BMC Bioinformatics *11*, 395.

Potting, C., Tatsuta, T., Konig, T., Haag, M., Wai, T., Aaltonen, M.J., and Langer, T. (2013). TRIAP1/PRELI complexes prevent apoptosis by mediating intramitochondrial transport of phosphatidic acid. Cell Metab *18*, 287-295.

Ruozi, B., Belletti, D., Tombesi, A., Tosi, G., Bondioli, L., Forni, F., and Vandelli, M.A. (2011). AFM, ESEM, TEM, and CLSM in liposomal characterization: a comparative study. International Journal of Nanomedicine *6*, 557-563.

Sebastián, D., Herrero, L., Serra, D., Asins, G., and Hegardt, F.G. (2007). CPT I overexpression protects L6E9 muscle cells from fatty acid-induced insulin resistance, Vol 292.
Segalés, J., Paz, J.C., Hernández-Alvarez, M.I., Sala, D., Muñoz, J.P., Noguera, E., Pich, S., Palacín, M., Enríquez, J.A., and Zorzano, A. (2013). A form of mitofusin 2 (Mfn2) lacking the transmembrane domains and the COOH-terminal end stimulates metabolism in muscle and liver cells. American Journal of Physiology - Endocrinology and Metabolism *305*, E1208-E1221.
Soriano, F.X., Liesa, M., Bach, D., Chan, D.C., Palacin, M., and Zorzano, A. (2006). Evidence for a mitochondrial regulatory pathway defined by peroxisome proliferator-activated receptor-gamma coactivator-1 alpha, estrogen-related receptor-alpha, and mitofusin 2. Diabetes *55*, 1783-1791.
Wu, Y., Wang, Y.Y., Nakamoto, Y., Li, Y.Y., Baba, T., Kaneko, S., Fujii, C., and Mukaida, N. (2010). Accelerated hepatocellular carcinoma development in mice expressing the Pim-3 transgene selectively in the liver. Oncogene *29*, 2228-2237.